PALS'15

September 22-25, 2015 Saratov, Russia

7th Finnish-Russian Photonics and Laser Symposium
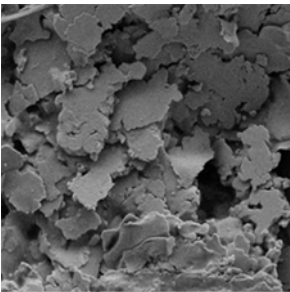
Programme and Book of Abstracts
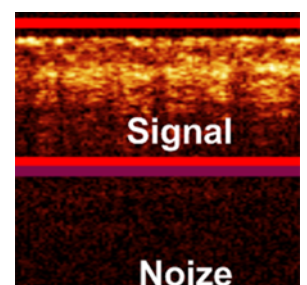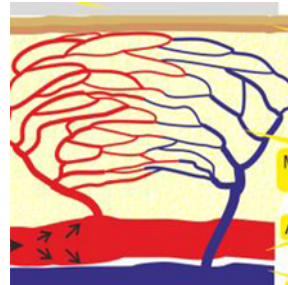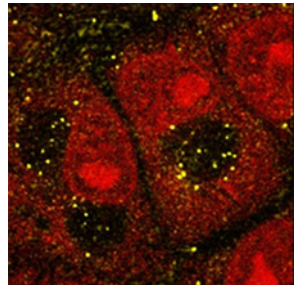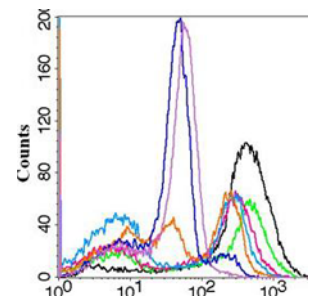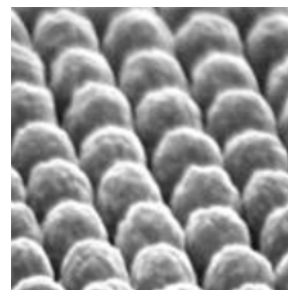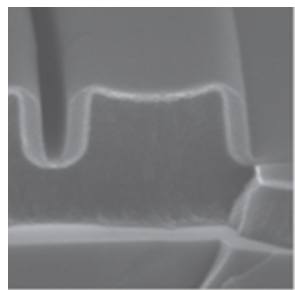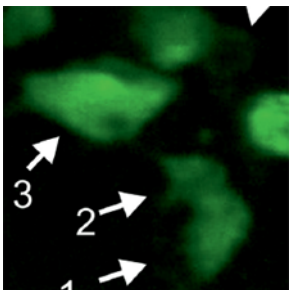
Photonics and Laser Symposium PALS'15
Organized by:
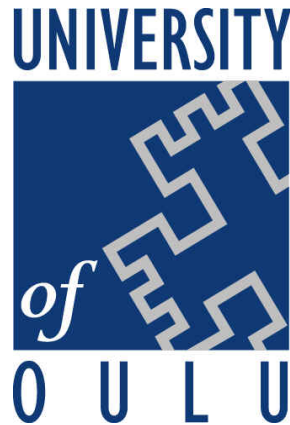
Saratov State University named after N.G. Chernyshevsky, Russia

University of Eastern Finland, Finland

International Laser Center of Lomonosov Moscow State University, Russia

University of Oulu, Finland

Institute of Biochemistry and Physiology of Plants and Microorganisms RAS

Europian Optical Society

Photonics and Laser Symposium PALS'15
Sponsored by:

LLC SPE Nanostructed Glass Technology, Russia

Russian Technology Platform "The Medicine of the Future", Russia

Russian Technology Platform "Photonics", Russia

RFBR – Russian Foundation for Basic Research

SPIE – The International Society of Photo-Optical Instrumentation Engineers, USA

LLC SPE Nanostructed Glass Technology, Russia

NT-MDT (Molecular Devises and Tools for Nanotechnology), Russia

Photonics and Laser Symposium PALS'15
With the help of:

OSA
The Optical Society

OBP
Research-Edicational
Institute of
Optics & BioPhotonics

SPIE. STUDENT CHAPTER
UNIVERSITY
OF OULU

SPIE. STUDENT CHAPTER
N.G. CHERNYSHEVSKY
SARATOV STATE
UNIVERSITY

Research-Educational Institute of Optics and Biophotonics at Saratov State University, Russia

SPIE University of Oulu Student Chapter

SPIE Student Chapter at SSU

OSA Student Chapter at SSU

In frames of the International Year of Light

UNESCO

INTERNATIONAL
YEAR OF LIGHT

Saratov State University Site Map

SSU Building III, 3rd floor

47 46
48 44 45
49
50
50a
51
Internet Session
52
54
55 58
56 57

SSU Library, 3rd floor

125 60 61 63 66 67
55 51 52
133 131
139 137
138

Library

Bldg. II

Moskovskaya str.

Bldg. I

Bldg. X

N
S

Universitetskaya str.

Bldg. III

Bldg. VIII

Bolshaya Kazatchia str.

Astrakhanskaya str.

Bldg. IX

Bldg. XI

Bldg. V
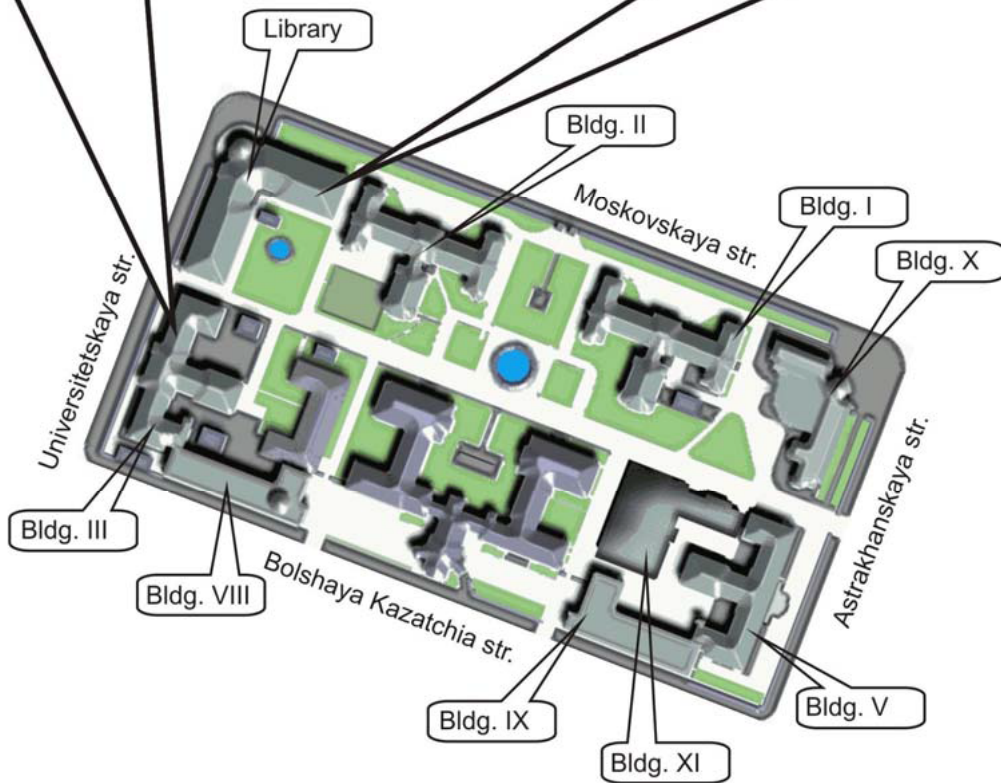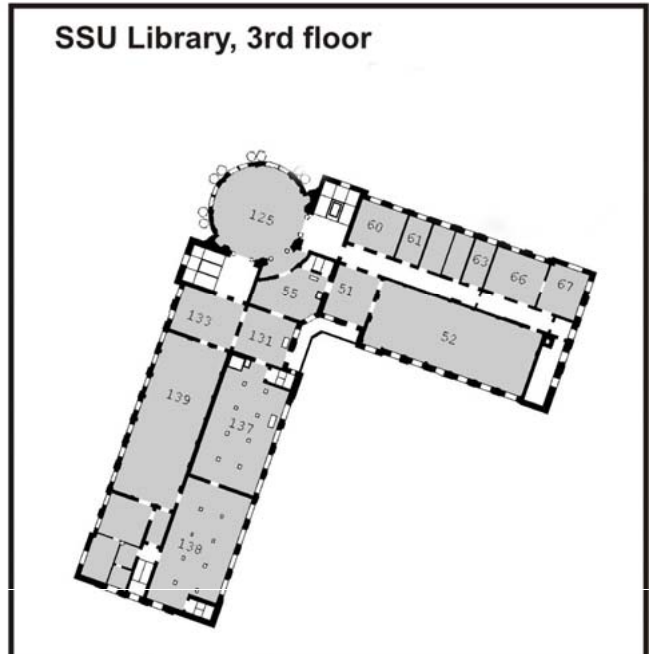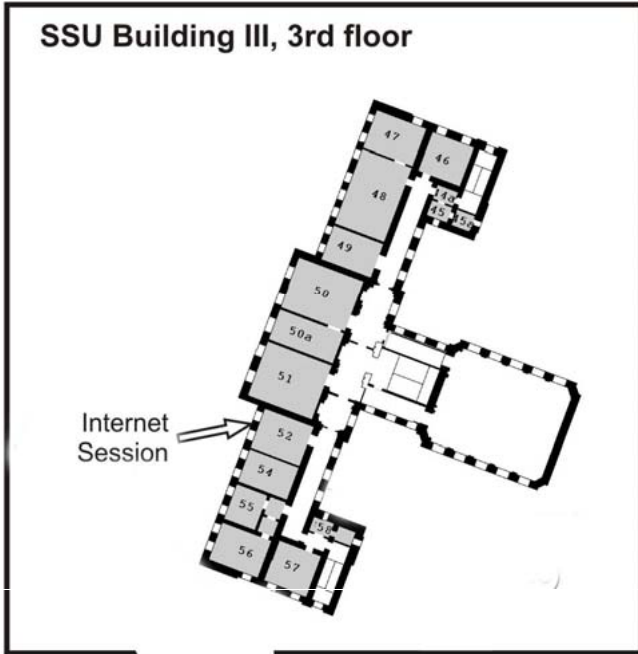
Committees

Honorary Chairs

Risto Myllylä,
University of Oulu, Finland

Yuri P. Svirko,
University of Eastern Finland, Finland

Co-Chairs

Vladimir A. Makarov,
Moscow State University, Russia

Timo Jääskeläinen,
University of Eastern Finland, Finland

Valery V. Tuchin,
Saratov State University, Russia

Committees

Secretary

Olga Bibikova,
University of Oulu, Finland
Saratov State University, Russia

Program Committee

Co-chairs
Alexander V. Priezzhev, Moscow State University, Russia

Igor V. Meglinski, University of Oulu, Finland

Members
Sergey M. Arakelian, Vladimir State University, Russia

Alexey N. Bashkatov, Saratov State University, Russia

Igor P. Gurov, Saint Petersburg National Research University ITMO, Russia

Seppo Honkanen, University of Eastern Finland, Finland

Martti Kauranen, Tampere University of Technology, Finland

Nikolai G. Khlebtsov, Institute of Biochemistry and Physiology of Plants and Microorganisms RAS

Jyrki Saarinen, University of Eastern Finland, Finland

Alexander M. Sergeev, Institute of Applied Physics RAS, Russia

Alexander P. Shkurinov, Moscow State University, Russia

Committees

Organizing Committee

Alexander V. Bykov, University of Oulu, Finland

Ivan V. Fedosov, Saratov State University, Russia

Elina A. Genina, Saratov State University, Russia

Mikhail Yu. Kirillin, Institute of Applied Physics RAS, Russia

Alexey P. Popov, University of Oulu, Finland

Polina A. Timoshina, Saratov State University, Russia

Daria K. Tuchina, Saratov State University, Russia

Yana V. Tarakanchikova, Saratov State University, Russia

Irina Yu. Yanina, Saratov State University, Russia/University of Oulu, Finland

Elena K. Volkova, Saratov State University, Russia/University of Oulu, Finland

Olga Izotova, Saratov State University, Russia

Welcome words from the Organaizers

Dear PALS'15 participants!

We are delighted to welcome you to the 7th Finnish-Russian Photonics and Laser Symposium-2015 and hope that you will have an exciting and inspiring time. The goal of the Symposium is to encourage and bring together both Russian and Finnish scientists, engineers and clinical researchers from variety of disciplines engaged in applying optical science, photonics and imaging technologies to problems in industry, biology and medicine. The scope of this bilateral symposium ranges from basic research to instrumentation engineering, biological and clinical studies. Browsing through this book of abstracts, you will find an impressive body of work in the talks and poster sessions.

Actually, the goal of PALS'15 is to continue and extend success of the previoussymposiaheldinSaratov(2003),Kajaani(2005),Moscow(2007), Tampere (2009), St. Petersburg (2011), and Kuopio (2013). Science in general and the symposium in particular is all about communicating and exchanging ideas. In this spirit of scientific exchange, we would like to thank you in advance for you active contribution to making the Symposium a success. We hope that while you are experiencing the exciting atmosphere of this event, you will gain new insights and learn about the fascinating new developments in Laser Physics, Photonics and Biophotonics.

With best wishes from the organizers,

Vladimir A. Makarov, Russian Co-Chair of the PALS'15

Timo Jääskeläinen, Finnish Co-Chair of the PALS'15

Valery V. Tuchin, Russian Co-Chair of the PALS'15

Programme

September 22, Tuesday		
9.00-14.00	**Registration**	*Building 3, Foyer*
14.00-14.10	**Opening of International Symposium "Optics and Biophotonics-III" and PALS-15** *Valery V. Tuchin*, Saratov State University *Timo Jääskeläinen*, University of Eastern Finland	*Building 10 Main Conf. Hall*
JOINT SFM/PALS PLENARY SESSION I (14.10-15.30) **Chair:** *Valery V. Tuchin*, Saratov State University, Russia		*Building 10 Main Conf. Hall*
14.10-14.50	**Delivery Systems: How to Delivery and to Activate at Time and Site Specific Manner** *Gleb B. Sukhorukov*, The Queen Mary University of London, UK; Saratov State University, Russia	
14.50-15.30	**Biophotonics on its Way into the Clinic,** *Juergen Popp*, Leibniz Institute of Photonic Technology, Jena, Germany	
15.30-16.00	**Coffee break**	
JOINT SFM/PALS PLENARY SESSION II (16.00-18.00) **Chair:** *Juergen Popp,* Leibniz Institute of Photonic Technology, Jena, Germany		*Building 10 Main Conf. Hall*
16.00-16.40	**Nonlinear Metasurfaces,** *ldar Gabitov*, Skolkovo Institute of Science and Technology, Moscow, Russia; University of Arizona, USA	
16.40-17.20	**Plasmonics Engineering for SERS Detection** *Nicolás Pazos-Pérez*, Centre Tecnologic de la Quimica de Catalunya, Spain	
17.20-18.00	**Fiber spectroscopy to detect tumor margins** *Viacheslav Artyushenko*, art photonics GmbH, Berlin, Germany; Prokhorov General Physics Institute, Russian Academy of Sciences, Russia	
18.00-18.30	**International Year of Light: Lighting the future: video from The National University of Ireland, Galway and Laser/Light Show "Fire Dance," Saratov**	
18.30-21.00	**Welcome party**	*Univ. camp.*

September 23, Wednesday	

JOINT SFM/PALS PLENARY SESSION III (9.00-10.00) **Chair:** *Alexander V. Priezzhev,* Lomonosov Moscow State University, Russia	*Building 10 Main Conf. Hall*

9.00-9.40	**Hybrid Plasmonic Nanoparticles and Atomic Clusters for Analytical and Theranostic Applications** *Nikolay G. Khlebtsov*, Institute of Biochemistry and Physiology of Plants and Microorganisms, Russian Academy of Sciences, Saratov State University, Russia
9.40-10.20	**Wavefront Imaging and Shaping Techniques for Biomedicine & Nanotechnology** *YongKeun (Paul) Park*, Department of Physics, KAIST, South Korea
10.20-10.50	**Coffee break**

INVITED LECTURE/ORAL PALS I SESSION (10.50-12.00) **Co-chairs:** *Timo Jääskeläinen,* University of Eastern Finland *Valery V. Tuchin,* Saratov State University, Russia	*Building 10, Hall 503*

10.50-11.10 Invited	**Interaction of visible light with blood vessels in human skin** *Alexey Kamshilin,* ITMO University, Russia
11.10-11.30 Invited	**FiDiPro Project on Biophotonics: Finland-Russian Collaboration** *Valery V. Tuchin*, Saratov State University; Institute of Precision Mechanics and Control RAS, Saratov; Interdisciplinary Laboratory of Biophotonics, Tomsk State University, Tomsk, Russia
11.30-11.45	**Implantable bio-markers for in vivo physiological assessment** *Anton Sadovoy*, Institute of Materials Research and Engineering, A*STAR, Singapore
11.45-12.00	**Investigation of bovine serum albumin glycation by THz spectroscopy** *Olga P. Cherkasova*, Institute of Laser Physics of SB RAS, Novosibirsk

INVITED LECTURE/ORAL PALS II SESSION (12.00-13.30) **Chair:** *Alexander V. Priezzhev,* Lomonosov Moscow State University, Russia		*Building 10, Hall 503*
12.00-12.20 Invited	**Parametric interaction of polarization singularities in isotropic chiral medium** *Igor A. Perezhogin,* International Laser Center of M.V. Lomonosov Moscow State University, Russia	
12.20-12.40 Invited	**Pulsed picosecond lasers with the dynamical operation control** *Nikita G. Mikheev,* International Laser Center and Physics Department of M.V. Lomonosov Moscow State University, Moscow, Russia	
12.40-13.00 Invited	**Monte Carlo simulations of optical brain imaging: Approaches, verifications, applications** *Mikhail Kirillin,* Institute of Applied Physics of RAS, Nizhny Novgorod, Russia; N. I. Lobachevsky State University of Nizhny Novgorod, Nizhny Novgorod, Russia	
13.00-13.15 Invited	**Quantified monitoring of skin OCT-image evolution under external action** *Pavel D. Agrba,* Lobachevsky State University of Nizhny Novgorod, Institute of Applied Physics of Russian Academy of Sciences, Russia	
13.30-14.30	**Lunch**	
15.00-17.00	**Social program (Volga boat trip)**	

September 24, Thursday	
SFM PLENARY SESSION V (9.20-10.00) **Chair:** *Dmitry A. Gorin, Saratov State University, Russia*	*Building 10 Main Conf. Hall*
9.20-10.00	**Silicon-iron Hybrid Nanoparticles with Optical, Luminescent and Magnetic Functionality** *Munir Nayfeh,* Department of Physics, University of Illinois at Urbana-Champaign, USA
JOINT INVITED/ORAL SESSION NANOBIOPHOTONICS I/ PALS III (10.00-11.00) **Chair:** *Nikolai G. Khlebtsov,* IBPPM RAS, Saratov State University, Russia	*Building 10 Main Conf. Hall*
10.00-10.20 Invited (PALS)	**Laser-induced semiconductor nano- microstructures with controlled topology: functional properties and verification of macroscopic quantum effects in thin-film and cluster** *Sergey Arakelian,*Vladimir State University named after A.G. and N.G. Stoletovs, Vladimir, Russia
10.20-10.40 Invited	**Super-resolution optical imaging and spectroscopy by scanning optical nano-antennas** *Pavel Dorozhkin*, NT-MDT Co., Russia
10.40-10.55	**Investigation of cell proliferative activity on the surface of the nanocomposite material produced by laser radiation** *Alexander. Gerasimenko*, National Research University «MIET», Russia
11.00-11.30	**Coffee break**
JOINT INVITED/ORAL SESSION NANOBIOPHOTONICS II/ PALS IV (11.30-13.00) **Chair:** *Nikolai G. Khlebtsov, I*BPPM RAS, Saratov State University, Russia	*Building 10 MainConf. Hall*
11.30-11.50 Invited (PALS)	**Application of atomic layer deposition in polymer based nanophotonic devices** *Seppo Honkanen,* **I**nstitute of Photonics, University of Eastern Finland, Joensuu, Finland
11.50-12.10 Invited (PALS)	**Generation of electromagnetic radiation in nano-structural matter** *Alexander Shkurinov*, Moscow State University, Moscow, Russia
12.10-12.25	**Efficient up-conversion phosphors on the basis of fluorides for photonics** *Sergey V. Kuznetsov*, Prokhorov General Physics Institute of Russian Academy of Sciences, Russia

12.25-12.40	**Up-conversion nanoparticles surface modification with photosensitizer molecules or gold nanoparticles for biomedical applications** *Daria Pominova,* General Physics Institute of the Russian Academy of Sciences, Russia
12.40-12.55	**Mechanisms of adsorption of nitrogenous bases on the surface of nanodiamonds** *Ekaterina Khusainova,* Moscow State University, Moscow, Russia
12.55-13.10	**The laser-ablative synthesis and the spectral-optical diagnostic of the ruby nanoparticles** *M.S. Baranov,* Volgograd State University, Volgograd, Russia
13.10-14.00	**Lunch**

INVITED/ORAL SESSION NANOBIOPHOTONICS III (14.00-16.00) **Chair:** *Nikolai G. Khlebtsov, I*BPPM RAS, Saratov State University, Russia	*Building 10 Main Conf. Hall*

14.00-14.15	**Comparative study on effectiveness of anticancer drugs conjugated with colloidal gold and phosphate dextran** *Artur Yu. Prilepskii,* IBPPM RAS, Saratov, Russia;
14.15-14.30	**A new synthetic approach to fine-tuning the wavelength of the gold nanorods' plasmon resonance**, *Sergey Semyonov,* Institute of Physical Chemistry and Electrochemistry, Russian Academy of Sciences, Russia
14.30-14.45	**Gold nanoparticles as PCR enhancers: Putative mechanisms study and biomedical applications** *Timofey Pylaev,* IBPPM RAS, Saratov, Russia;
14.45-15.00	**Formation of functional calcium carbonate coatings on polymeric fibers for biomedical applications** *Marya Savelyeva,* Saratov State University, Russia
15.00-15.15	**Optical properties of monodisperse gold nanoshells** *Vitaly Khanadeev,* IBPPM RAS, Saratov, Russia; Saratov State University, Saratov, Russia;
15.15-15.30	**Microcapsules based on carbon nanotubes and gold nanoparticles as multimodal photoacoustic and SERS platform** *Alexey Yashchenok,* Remote Controlled Theranostic Systems Lab, Institute of Nanostructures and Biosystem, Saratov State University, Russia;

15.30-15.45	**Porous calcium carbonate submicron particles for the photosensitizer encapsulation** *Yulia Svenskaya*, Saratov StateUniversity, Saratov, Russia;	
15.45-16.00	**Analyzing Raman spectra from the first principles** *Daniil Bratashov*, Saratov State University, Russia;	
JOINT SFM/PALS POSTER/INTERNET SESSION AND INTERNET DISCUSSION (17.30-19.30) **Moderators:** *Dmitry Agafonov, Ivan V. Fedosov,* Saratov State University, Russia		*Building 3, 3d floor Hall*
September 25, Friday		
JOINT INVITED LECTURE/ORAL SESSION MICROSCOPY AND LOW-COHERENCE METHODS/ PALS V (9.00-11.00) **Chair:** *Kirill V. Larin,* University of Houston, USA		*Building 10 Main Conf. Hall*
9.00-9.20 Invited (PALS)	**Addressed thermogenetic activation of cells by infrared and microwave radiation** *Andrei B. Fedotov,* Physics Department, International Laser Center, M.V. Lomonosov Moscow State University, Moscow, Russia; Russian Quantum Center, Moscow Region	
9.20-9.35 (PALS)	**Effects of cisplatin on the level of hydrogen peroxide and cell death in HeLa Kyoto cells** *Anastasya S. Belova*, Institute of Applied Physics of the Russian Academy of Sciences, Nizhny Novgorod, Russia; Lobachevsky State University of Nizhni Novgorod, Nizhni Novgorod, Russia	
9.35-9.50	**Vessel-contrast enhancement in label-free optical coherence angiography based on phase and amplitude speckle variability** *Lev A. Matveyev,* Institute of Applied Physics RAS, Russia	
9.50-10.05	**Stochastic optical reconstruction microscopy (STORM) image restoration from subsets of localizations insufficient for Nyquist criterion** *Alexander Moiseev*, IAP RAS, Russia	
10.05-10.20	**Digital holography methods for optical aberrations measurement and compensation** *Vasiliy Matkivskiy***,** IAP RAS, Russia	

10.20-10.35	**Analysis of dynamics of a caspase-3 activity in cancer cells during apoptosis using FLIM/FRET technique** *Tatiana F. Sergeeva,* Nizhny Novgorod State Medical Academy, Russia

INVITED LECTURE/ORAL PALS VI SESSION (9.00-11.00) **Chair:** *Sergey M. Arakelian,* Vladimir State University, Russia		*Building 10, Hall 503*
9.00-9.20 **Invited**	**Superfilamentation in water with tight focusing laser beams: from femtoseconds to microseconds** *Fedor V. Potemkin,* Faculty of Physics and International Laser Center M. V. Lomonosov Moscow State University, Moscow, Russia	
9.20-9.40 **Invited**	**Photo-induced phenomena in chalcogenide glasses irradiated by high-intensity laser pulses** *Elena Romanova,* Saratov State University, Saratov, Russia	
9.40-9.55	**Calibration of miniature prism-based stereoscopic imagers for precise spatial measurements** *Alexey Gorevoy,* Scientific and Technological Center of Unique Instrumentation of Russian Academy of Sciences, Moscow, Russia	
9.55-10.10	**Acousto-optical method for full-field high temperature measurement** *Alexander S. Machikhin,* Scientific and Technological Center of Unique Instrumentation of Russian Academy of Sciences, Moscow, Russia	
10.10-10.25	**Raman scattering and fluorescence of graphitic phases from B-C-N triangle** *Pavel V. Zinin,* Russian Academy of Sciences, Moscow, Russia	

11.00-11.30	**Coffee break**

JOINT INVITED LECTURE/ORAL SESSION BIOPHYSICS III/ PALS VII (11.30-13.00) **Chair:** *Ivan V. Fedosov,* Saratov State University, Russia		*Building 10 Main Conf. Hall*
11.30-11.50 **Invited**	**The regularizing functional minimization based reconstruction of tissue scattering inhomogeneities from time-resolved optical projections** *Alexander B. Konovalov,* Russian Federal Nuclear Center - Zababakhin Institute of Apllied Physics, Russia	

11.50-12.10 Invited	**SA robust method of strain mapping in compressional optical coherence elastography using combined sub-wavelength phase-resolved measurements and pixel-scale displacement tracking** *Vladimir Y. Zaitsev,* Institute of Applied Physics RAS, Russia
12.10-12.30 Invited (PALS)	**Mechanisms of tissue optical immersion clearing** *Genina Elina*, Saratov State University, Russia
12.30-12.45	**Neoplasms treatment by diode laser with and without real time temperature control on operation zone** *Andrei V. Belikov*, ITMO University, Saint Petersburg, Russia
12.45-13.00	**Study of human skin neoplasms with autofluorescence method in NIR region** *Julia A. Khristoforova*, Samara State Aerospace University, Russia
14.00-17.00	**Round-table discussions and closing of the School and The Symposium**

September 24, Thursday
POSTER SESSION (17.30-19.30)
Chair:
Olga Bibikova, University of Oulu, Finland; Saratov State University, Russia

1RF. **Iridium nanopillar arrays for highly reproducible surface-enhanced Raman spectroscopy (SERS)**
Antti Matikainen, Institute of Photonics, University of Eastern Finland

2RF. **From silver chloride intermediate to sers applications** *Tarmo Nuutinen*, Institute of Photonics, University of Eastern Finland, Joensuu, Finland; Department of Biology, University of Eastern Finland, Joensuu, Finland

3RF. **The effect of viscosity on the thermal stability of coupled multi-enzyme system lactate dehydrogenase + NAD(P)H:FMN-oxidoreductase+bacterial Luciferase**
Maria S. Nemchinova, Department of Biophysics, Institute of Fundamental Biology and Biotechnology, Siberian Federal University, Krasnoyarsk, Russia

4RF. **UV laser-induced fluorescence spectroscopy and laser-Doppler flowmetry in the diagnostics of alopecia**
Diana P. Skomorokha, Krasnoyarsk State Medical University named after Prof. V.F. Voino-Yasenetsky, Krasnoyarsk, Russia

5RF. **Surface-enhanced Raman spectroscopy for enzymatic activity detection**
Natalia L. Nechaeva, Chemical enzymology department, Faculty of Chemistry, Lomonosov Moscow State University, Russia

6RF. **Plasmon-resonant nanoparticles with variable morphology for optical imaging**
Olga Bibikova, University of Oulu, Oulu, Finland, Saratov State University, Saratov, Russia

7RF. **The morphological changes in transplanted tumors of rats at plasmonic phothothermal therapy**
Alla B. Bucharskaya, Saratov State Medical University, Russia; Research-Educational Institute of Optics and Biophotonics, Saratov

8RF. **Monitoring properties of biological tissues using [Y2O3:Yb, Er] upconversion particles**
Elena Volkova, Saratov State University, Research-Educational Institute of Optics and Biophotonics, Russia; University of Oulu, Finland

9RF. Multimodal coherent nonlinear raman microspectroscopy by chirped ultrashort laser pulses
Alexander Lanin, Faculty of Physics, International Laser Center, Moscow State University Moscow, Russia; Russian Quantum Center, Moscow State University, Moscow, Russia

INTERNET SESSION (17.30-19.30)

Invited
1. Improvement of upconversion deep-tissue imaging with optical clearing
Alexey P. Popov, Optoelectronics and Measurement Techniques Laboratory, University of Oulu, Oulu, Finland

Invited
2. Optical properties of tissues in the visible– NIR spectral range
Alexey N. Bashkatov, Research-Educational Institute of Optics and Biophotonics, Saratov State University, Saratov, Russia; Interdisciplinary Laboratory of Biophotonics, Tomsk State University, Tomsk, Russia

Invited
3. Experience in collaborative construction and biomedical applications of laser tweezers
Alexander Priezzhev, Laser Biomedical Photonics Laboratory, Physics Department; Intertational Laser Centre, Lomonosov Moscow State University, Moscow, Russia

Abstracts

INTERACTION OF VISIBLE LIGHT WITH BLOOD VESSELS IN HUMAN SKIN

Alexei A. Kamshilin

ITMO University, 197101 St. Petersburg, Russia

alexei.kamshilin@yandex.ru

The skin is highly dynamic organ capable to respond on the variable environment. Consequently, the optical properties of skin are also dynamic. Here, we shall concentrate our attention on the relatively fast dynamic changes of the light parameters occurring at the heartbeat frequency which is typically about 1 Hz for a subject at rest. Recently, many groups reported about possibility to study the cardiovascular processes in-vivo and noninvasively by analysing conventional video recordings and extracting from them the areas that are modulated in time at the heart rate [1-3]. Many researchers reported that the highest signal-to-noise ratio of the pixels modulation was observed under illumination the tissue by the green light [1-5]. This observation deserves deep discussion, which will be presented in the report.

Human skin has a complex layered structure containing three main layers: Stratum Corneum (10-20 μm, dead cells), Epidermis (100-150 μm, gel-like substance without blood vessels), and Dermis (3-4 mm, comprising upper capillaries and deeper vascular plexus). Visible light may enter the epidermal and dermal layer where it can be absorbed and/or scattered. Light absorption by the haemoglobin and water in the dermis define the absorption parameters of the whole skin. Temporal modulation of the light after its interaction with the dermis is usually explained by pulsatile variations of the optical density due to blood-volume pulsations in the arteries [6]. Blood volume change in capillaries and veins during the time of one cardiac cycle (about 1 s) is considered insignificant [7]. This explanation is hardly applied to the case of green light (525 nm) because its penetration depth into the skin was estimated to be between 0.3 and 0.9 mm [8,9], while the arteries are typically situated more than 3 mm below the stratum corneum in the wrist, and more deeper in the palm [10].

This contradiction was resolved in new model of light interaction with the skin recently proposed in our group [11], which emphasizes the role of elastic deformations of the dermis by pulsating arteries. According to this model, pulse oscillations of the arterial transmural pressure, which occur during every cardiac cycle, deform the connective-tissue components of the dermis. Growing transmural pressure of the arteries during the systole compresses the connective tissues of the dermis in a local place, which results in the increasing density of capillaries. Therefore, the light propagating through this place will be stronger both absorbed and scattered. Consequently, the power of the light remitted to the video camera or photodiode will be modulated inversely proportional to the degree of the dermis compression.

Figure 1 shows a simplified concept of the proposed model. In the end-diastole phase (Fig. 1a), the arterial pressure is at its minimum resulting in the smallest artery size, which applies minimal stresses to the dermis. Then the fast growing arterial pressure during the systole provides the force which compresses the dermis depending on the status of the stratum corneum. If the subject's skin is highly elastic (which is typical for young persons), the enlargement of the artery leads to reshaping of the skin surface with moderate compression of the dermis as shown in Fig. 1b. In contrast, when the skin movement is limited by a mechanical contact (Fig. 1c) the dermis is significantly compressed, which leads to higher density of capillaries. Both the absorption and scattering coefficient of the compressed tissue grows up resulting in diminishing of the remitted

light intensity. Therefore, arterial pulsations can be indirectly monitored even by using the light, which slightly penetrates into the biological tissue.
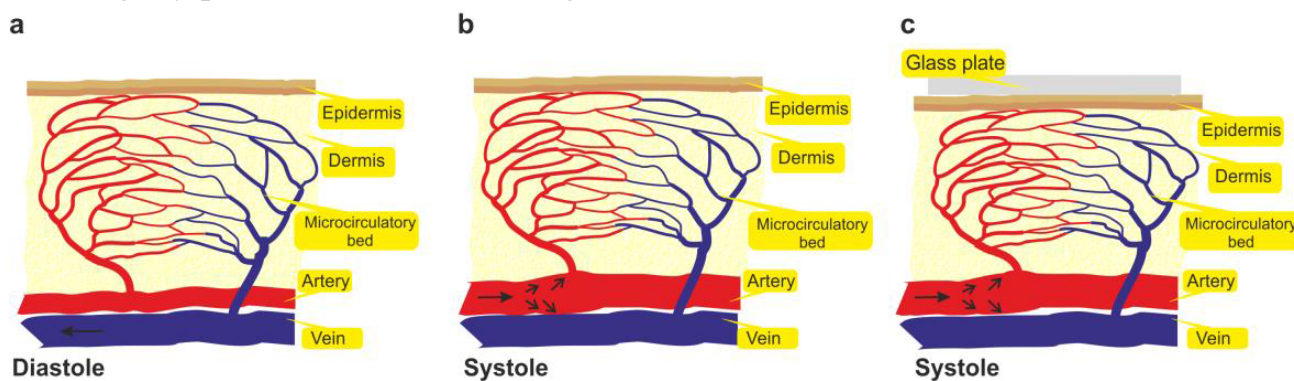
Fig. 1. Simplified drawing of a new model of the light interaction with the dermis.

In the presentation we will demonstrate observation the counter-phase modulation of the light power remitted from adjacent areas of the skin and strong influence of the external contact on the temporal shape of the light-power modulation. These data cannot be explained in the frames of the conventional photoplethysmography model but they find reasonable explanation in the new model [11].

[1] W. Verkruysse, L. O. Svaasand, and J. S. Nelson, Opt. Express 16, 21434 (2008).

[2] A. A. Kamshilin, S. V. Miridonov, V. Y. Teplov, R. Saarenheimo, and E. Nippolainen, Biomed. Opt. Express 2, 996 (2011).

[3] U. Bal, Biomed. Opt. Express 6, 86 (2015).

[4] B. A. Fallow, T. Tarumi, and H. Tanaka, J. Clin. Monit. Comput. 27, 313 (2013).

[5] A. A. Kamshilin, V. Y. Teplov, E. Nippolainen, S. V. Miridonov, and R. Giniatullin, PLoS ONE 8, e57117 (2013).

[6] J. Allen, Physiol. Meas. 28, R1-R40 (2007).

[7] Y. C. Fung, B. W. Zweifach, and M. Intaglietta, Circ. Res. 19, 441 (1966).

[8] R. R. Anderson and J. A. Parrish, in: The Science of Photomedicine, J. D. Reganand and J. A. Parrish, eds., (Springer US, New York, 1982), Ch. 6.

[9] A. N. Bashkatov, E. A. Genina, V. I. Kochubey, and V. V. Tuchin, J. Phys. D 38, 2543 (2005).

[10] H. Gray, Anatomy of the human body (Elsevier, Edinburgh, 2008).

[11] A. A. Kamshilin, E. Nippolainen, I. S. Sidorov, P. V. Vasilev, N. P. Erofeev, N. P. Podolian, and R. V. Romashko, Sci. Rep. 5, 10494 (2015).

ADDRESSED THERMOGENETIC ACTIVATION OF CELLS BY INFRARED AND MICROWAVE RADIATION

A.B.Fedotov,[1,2] I.V.Fedotov,[1,2] A.A.Lanin,[1,2] D.I.Kulik,[1] N.A.Safronov,[1] Yu.G.Ermakova,[3] M.E.Matlashov,[3] D.A.Sidorov-Biryukov,[1,2] V.V.Belousov,[3] A.M.Zheltikov[1,2,4]

[1]*Physics Department, International Laser Center, M.V. Lomonosov Moscow State University, Moscow 119992, Russia*

[2]*Russian Quantum Center, ul. Novaya 100, Skolkovo, Moscow Region, 143025 Russia*

[3]*M.M. Shemyakin and Yu.A. Ovchinnikov Institute of Bioorganic Chemistry, Russian Academy of Sciences, Moscow 117997, Russia*

[4]*Department of Physics and Astronomy, Texas A&M University, College Station TX 77843, USA*

New technologies enabling a high-precision control over the electrical activity of specific cells in a living organism offer unique opportunities for the functional analysis of complex biological systems, including brain and its functions. Optogenetics is revolutionizing neuroscience through the use of genetically encoded light-sensitive ion channels [1-2], which enable a spatially precise selective modulation of specific cells within complex distributed networks of neurons, thus offering unique tools for studying the mechanisms whereby the dynamics of these networks controls cognitive responses, memory, learning, and behavior. As a promising alternative, thermogenetics uses thermosensitive ion channels [3-5]. However, applications of thermogenetics in neuroscience studies are limited by the lack of tools enabling a precisely controlled, well-localized control of temperature inside living systems, which would prevent heating that would be incompatible with the general physiology of the organism and help avoid increased background activity of cells. In our work, we demonstrate a thermogenetic activation of individual cells in a cell culture using microwave and infrared radiation.
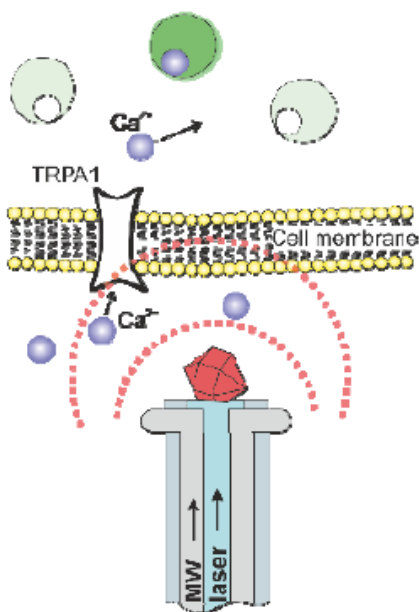
Fig. 1. Local heating and thermometry of cells thermosensitive TRP channels and Ca2+ indicators.

In the experiments with microwave field, it was delivered to a region of interest through a miniature microwave transmission line, which consists of a pair of copper wires 50 μm in diameter each, running along the optical fiber and short-circuited with an open-ring section, winding around the fiber tip (Fig.1). The microwave-induced heating of the cell culture gives rise to a rapidly decaying temperature gradient, which confines thermogenetic activation to cells adjacent to the open-ring microwave antenna (Fig.1). Moreover, a microwave transmission line is integrated with an optical fiber and was used for online local temperature measurements.

Our "thermometer" was performed by using the temperature-dependent frequency shift of optically detected magnetic resonance [6], which is induced by coupling the microwave field, delivered by the microwave transmission line, to nitrogen--vacancy (NV) centers in diamond on the tip of the fiber probe (Fig.1).Experiments on thermogenetic control and thermometry of cells were performed on a culture of Human Embryonic Kidney 293 (HEK-293) cells grown in a Petri dish. The HEK-293 cells were transfected with vectors expressing Green-GECO calcium indicator and rattlesnake TRPA1 channels, known to be responsible for remote thermosensation by rattlesnake Crotalus atrox..Cell imaging was performed using a 10x microscope objective and a CCD camera. The cells were irradiated with a continuous-wave 473-nm diode-laser output, which provided optical excitation of Green-GECO. We have demonstrated and investigated a thermogenetic activation of individual cells with a microwave field delivered to the cells of interest through a miniature microwave transmission line. Fig.2 shows an example of thermal response of a group of seven cells (labelled with arrows in the image) located within a distance of 120 μm from the openring microwave antenna on the tip of the fiber probe, with the nearest cell (cell 1) lying at a distance of about 60 μm from this antenna labeled with arrows in Fig.2 [7].
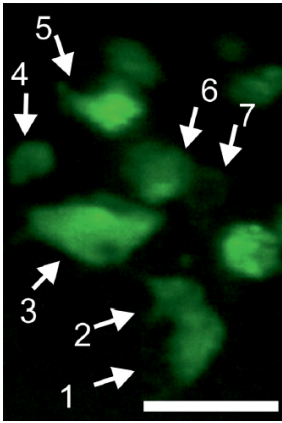
Fig. 2. An image of a group of seven HEK-293 cells expressing the rattlesnake TRPA1 channel and Green-GECO calcium indicator in a cell culture exposed to microwave radiation. The scale bar is 50 mm.

To investigate addressed heating of the transfected neuron cells with TRPA1 channels by infrared radiation, we used femtosecond optical parametric oscillator (pumped by Coherent HP Mira femtosecond laser) which allows getting tunable radiation at wavelengths from 1.0 to 1.5 μm. The infrared radiation could be focused to a spot with the diameter about 40 μm, that guaranteed heating of single cell. The same diamond quantum thermometer was explored for local temperature control. Thus, we have shown effective and reproducible activation of TRPA1 channels in individual neuron cells by infrared radiation, that was visualized by increasing in calcium flow through activated TRPA channels.

[1] K. Deisseroth, Nat. Methods. 8, 26 (2011).
[2] G. Miesenbock, Science. 326,395 (2009).
[3] J.G. Bernstein, P.A.Garrity, and E. S. Boyden, Curr. Opin. Neurobiol. 22, 61 (2012).
[4] G.M.Story, A.M.Peier, A.J. Reeve, S.R. Eid, et al., Cell. 112, 819 (2003).
[5]. E.O.Gracheva, N. T. Ingola, Y. M. Kelly, et al., Nature, 464, 1006 (2010).
[6] G. Kucsko, P. C. Maurer, N. Y. Yao, M. Kubo, et al., Nature 500, 54–58 (2013).
[7] N.A.Safronov, I.V. Fedotov, et al., Appl. Phys. Lett., 106, 163702 (2015).

IMPLANTABLE BIO-MARKERS FOR IN VIVO PHYSIOLOGICAL ASSESSMENT

Anton Sadovoy[1], Anton Gurkov[2], Cathleen Teh[3], Maxim Timofeyev[2], Igor Meglinski[4]

[1]*Institute of Material Research and Engineering, A*STAR, Singapore*

[2]*Institute of Biology, Irkutsk State University, Russia*

[3]*Institute of Molecular and Cell Biology, A*STAR, Singapore*

[4]*University of Oulu, Optoelectronics and Measurement Techniques Laboratory, Finland*

sadovoyav@imre.a-star.edu.sg

In vivo sensors for rapid quantification and analyze of physiological changes in mammalians and other organisms is the major challenge in biological and ecological express screenings [1]. The wide range of chemical sensors and assays for detection of some of parameters like pH, oxygen, temperature, and glucose are presented on the market [2]. Usually the sensors are applied in solution for ex vitro test or as an injection for in vivo test. To overcome spreading of sensors around organism and sometimes toxicity of assays we presenting novel type of implantable bio-markers for in vivo assessment of physiological parameters.

Polyelectrolyte multilayer (PM) capsules have shown a few promising applications as a container for biosensors [3-5] since they were fist obtained in 1998 Max Plank Institute of Colloids, Germany [6]. The PM encapsulation technique is based on layer-by-layer adsorption of oppositely charged polyelectrolytes on micron- or sub-micron size cores. Fluorescence assays usually preloaded in the cores are released inside the microcapsules after them dissolving. That the process of layer adsorption is water based makes it more biological friendly.

Recently we demonstrated possible application of PM capsules as a promising container for implantable bio-sensors [7]. Here we are presenting a new step of in vivo assessment of pH level in zebrafish larvae (Fig. 1). Also the change of pH level after applying of external stress condition was clearly demonstrated. Developed technique could find wide application not only in bio-imaging but also in meat production.

Fig. 1 Brain-ventricle injection of encapsulated pH-sensor and signal evaluation

[1] Paul, D. 'O, Clinica Chimica Acta. 2011, 412, 1749-1761.

[2] Moczko, E., Meglinski, I. V., Bessant, C., and etc., Analytical Chemistry. 2009, 81, 2311-2316

[3] Kreft, O.; Javier, A. M.; Sukhorukov, G. B.; Parak, W. J. Journal of Materials Chemistry 2007, 17, 4471-4476

[4] De Geest, B. G.; De Koker, S.; Sukhorukov, G. B.; Kreft, O.; Parak, W. J.; Skirtach, A. G.; Demeester, J.; De Smedt, S. C.; Hennink, W. E. Soft Matter 2009, 5, 282-291

[5] McShane, M. J.; Brown, J. Q.; Guice, K. B.; Lvov, Y. M. Journal of Nanoscience and Nanotechnology 2002, 2, 411-416

[6] Donath, E.; Sukhorukov, G. B.; Caruso, F.; Davis, S. A.; Mohwald, H. Angewandte Chemie-International Edition 1998, 37, 2202-2205

[7] Sadovoy A.V., Teh C., Korz V., and etc., Laser Physics Letters. 2012, 9, 542–546

INVESTIGATION OF BOVINE SERUM ALBUMIN GLYCATION BY THZ SPECTROSCOPY

O. P. Cherkasova[1], M. M.Nazarov[2], A. P. Shkurinov[2, 3]

[1]*Institute of Laser Physics of SB RAS, Novosibirsk, 630090 Russia*

[2]*Institute on Laser and Information Technologies of RAS, Shatura, 140700 Russia*

[3]*Lomonosov Moscow State University, Moscow, 119991, Russia*

o.p.cherkasova@gmail.com

THz spectroscopy is widely used in the study of protein conformation. Protein glycation is a non-enzymatic reaction between the carbonyl groups of monosaccharides such as glucose and fructose with the amino groups of proteins, for example albumin. The reaction initiates a complex cascade of protein modifications resulting in loss of both secondary and tertiary structure [1]. The glycation process is accelerated under hyperglycemic conditions. Albumin glycation alters ligand binding and plays a significant role in diabetic complications.

We used THz spectroscopy to study glycation dynamics of bovine serum albumin (BSA). The experiments were made in the transmission geometry. This method is more accurate to determine the properties of the solution at low frequencies. BSA (50.0 mg/ml) was incubated with 0.5M glucose (or fructose) in 50 mM phosphate buffer, pH 7.4, for 0-96 h at 47°C.

It was found that amplitude of albumin THz absorption depends on type of sugars and incubation time (fig.1). Moreover, changes were more pronounced in the case of fructose. The absorption spectra of BSA incubated in buffer alone did not change significantly.
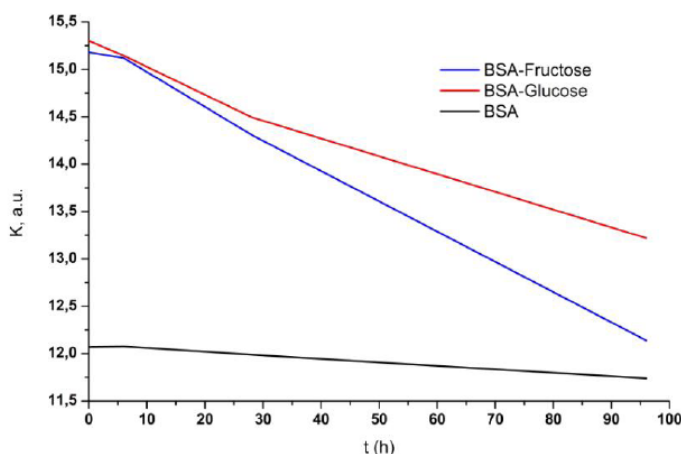
Fig. 1. K- coefficient calculated from THz transmission spectra, t – incubation time (h)

These results show that THz spectroscopy is a useful tool for study of protein glycation in time.

[1] G. Fanali, A. Masi, V. Trezza, M. Marino, M. Fasano, Molecular Aspects of Medicine, 33, 209 (2012).

PARAMETRIC INTERACTION OF POLARIZATION SINGULARITIES IN ISOTROPIC CHIRAL MEDIUM

I. A. Perezhogin[1], K.S. Grigoriev[2], V.A. Makarov[1,2]

[1]International Laser Center of M.V. Lomonosov Moscow State University, Russia

[2]Faculty of Physics of M.V. Lomonosov Moscow State University, Russia

iap1@mail.ru

In the present study we consider the polarization singularities evolution in parametric nonlinear processes. At the present time two general types of polarization singularities appearing in a beam propagating in 3D-space are known: surfaces of linear polarization (L-surfaces) and lines of circular polarization (C-lines) [1]. C-lines intersect the transversal planes of a beam at points of purely circular polarization (C-points), embedded into the inhomogeneous distribution of elliptic polarization. The orientation of the polarization ellipse is undefined in a C-point, which is provided by a phase singularity (vortex) of one of the circularly polarized components of the light beam in this point. Every singular point, and, consequently, C-line, has its topological charge determined by the number of full rotations of polarization ellipse calculated along small closed loop around the singularity (similarly to the topological charge of the optical vortex). Polarization singularities are vector analogues of optical vortices and their applications include scattering media diagnostics (by a statistical approach to singularities), soliton formation, telecommunications, obtaining of entangled quantum states, optical traps and complex field distributions for manipulating and trapping of small particles.

In parametric nonlinear processes the formation and the evolution of such field distributions can be controlled via the polarization state, frequencies and geometric parameters of the incident beams, analogously to the methods used in parametric processes with "scalar" (linearly and uniformly polarized) optical vortices. This gives one a flexible tool to control the structure of polarization singularities for different applications.

In our present study we consider sum-frequency generation in the bulk of isotropic chiral medium by bichromatic light field containing initially one polarization singularity, and degenerate case of this problem, when we consider the reflected radiation at double frequency, appearing due to the bulk nonlocal response and surface response of the medium.

In case of bulk sum-frequency generation the fundamental beams in question are Gaussian beam with elliptic polarization at one of the fundamental frequencies and Laguerre-Gaussian beam with right-hand circular polarization at another fundamental requency. The second beam has a phase singularity on its axis. Nonlinear mixing of the fundamental beams leads to the formation of complex distribution of medium's nonlinear polarization field. Being inhomogeneously polarized, this field contains several C-lines, and their total topological charge depends only on the eccentricity of the Laguerre-Gaussian beam polarization ellipse and the ratio of the wave numbers of two fundamental beams. Two types of configurations are considered: 1) C-lines of the signal beam have spiral structure; the handedness of a spiral depends on the sign of the wave-vector mismatch, and the mean "step" of a spiral is reversely proportional to its absolute value; 2) all C-lines in the signal beam form loops, but depending on the wavevector mismatch the number and shape of the loops are different.

In case we consider the second harmonic generation (degenerate case of sum-frequency eneration),

the local quadratic optical susceptibility of the medium bulk does not give any contribution to the double frequency signal while the nonlocal one provides it only under special conditions [2]. So, it is reasonable to consider reflected signal at double frequency, appearing both due to the nonlocal bulk contribution and surface contribution of the medium, as it was done in [3]. We consider the same structure of the incident beam being the superposition of Gaussian and Laguerre-Gaussian modeshaving polarization with opposite rotation handedness.

In case of purely bulk nonlinearity the signal beam contains two C-points with total topological charge equal to doubled charge of the initial singularity. However, their polarization handedness is not reversed if the C-point in the fundamental beam has negative charge. Media with both bulk and surface response generate far more complicated polarization patterns of the signal beam, which in special cases inherit the symmetry of the fundamental beam (fig. 1). Total topological charges of left-handed and right-handed C-points depend only on the charge of the initial C-point, but do not reflect the difference between its "lemon" and "monstar" patterns. For the media with both bulk and surface nonlinear response total topological charge may not be equal to doubled charge of the initial C-point.
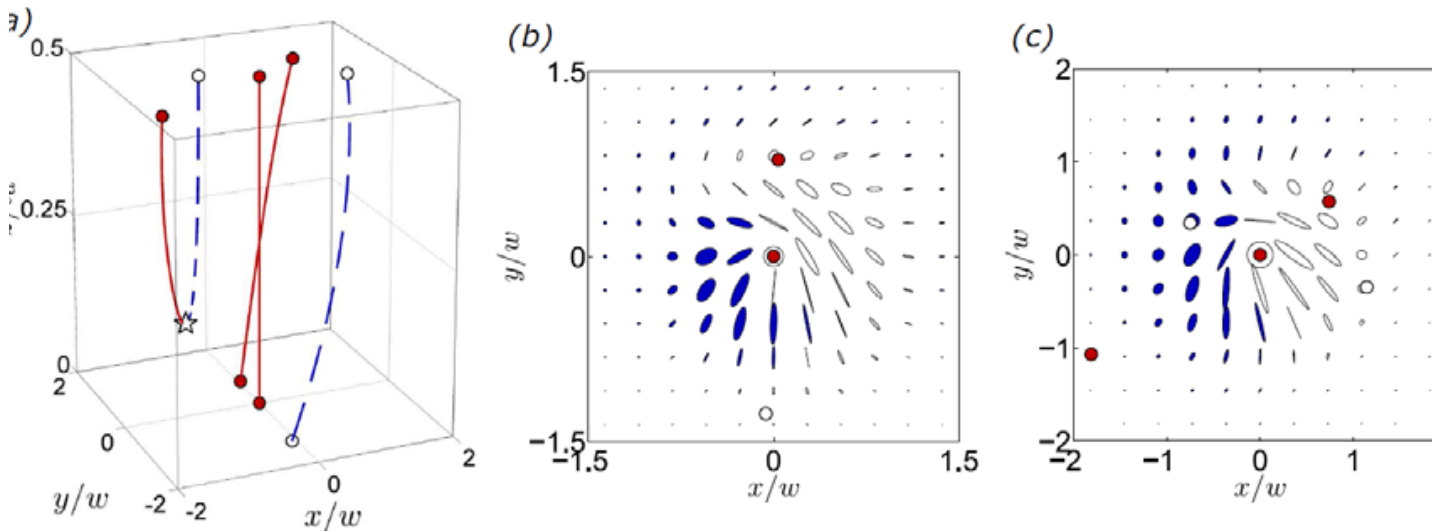
Fig. 1. C-lines in propagating reflected beam (a) and its transversal polarization distributions in the reflected beam at double frequency on the medium surface (b) corresponding to bottom slice of (a) and at half of the diffraction length from the medium surface (c) corresponding to top slice of (a). Red solid lines in (a) and red markers in (a – c) correspond to C-lines/points with positive topological charge ('lemon'and 'monstar') while blue dashed lines and white (empty) markers correspond to C-lines/points with negative topological charge. Star in (a) indicates the place of birth of two C-points with opposite topological charges. Empty and shaded ellipses indicate different handedness of polarization rotation. In the considered case the medium possesses both bulk and surface quadratic optical response.

[1] J. F. Nye. Proceedings of the Royal Society of London A: Mathematical, Physical and Engineering Sciences 389 (1983) 279–290.
[2] S.N. Volkov, N.I. Koroteev, V.A. Makarov. Journal of Experimental and Theoretical Physics 86 (1998) 687-695.
[3] N.I. Koroteev, V.A. Makarov, S.N. Volkov, Laser Phys. 8 (1998) 532–535.

PICOSECOND LASERS WITH THE DYNAMICAL OPERATION CONTROL

N.G.Mikheev, V.B.Morozov, A.N.Olenin, D.V.Yakovlev

International Laser Center and Physics Department of M.V. Lomonosov Moscow State

University, Moscow 119992, Leninskiye Gory

ng.mikheev@physics.msu.ru

Highly effective, compact and robust picosecond lasers with high enough single pulse energy of millijoule level and more, reasonably high and controllable repetition rates up to a few kilohertz are claimed for the implementation of different schemes of time-resolved laser spectroscopy, satellite and lunar laser ranging, precision micromachining, optical pump of parametric amplifiers, driving photoinjectors of electron accelerators and mw-guns. Using pulsed (or pulsed-periodic) solid-state laser schemes is most relevant for these purposes. Advanced pulsed lasers of ultrashort, mainlly picosecond, pulses may use operation control schemes based on active or passive mode locking, negative feedback and adjustable loss level in the resonator [1]. At the integration into complicated measuring systems and technological complexes, main advantages of picosecond lasers can be linked to the possibility of obtaining high values of energy and peak power just at the output of the laser at a sufficiently compact design, high stability of parameters, low sensitivity to operating conditions, with the simplicity of implementation of powerful amplifier stages [2] as well as with low optical jitter value [3].

In pulse regime, preparation of each laser shot evolves from the noise level and phase connection between the generated pulses is absent. This makes inapplicable the schemes of precise frequency and phase stabilization, designed for continuous femtosecond laser systems. At the same time, in the case of pulsed laser action one may raise an issue of implementation of moderately precise (within a fraction of the time idth) but rather quickly realized synchronization, carried out during the development of the next generated pulse (microsecond scale). The successful solution of this problem is related to the detailed experimental and theoretical study of the of laser pulse formation.

Models describing the evolution of time pulse profile in lasers with active and passive mode-locking were proposed in [4]. The equations can be solved analytically in the cases of purely active or purely passive mode locking. Even under the joint action of two mechanisms, only numerical solution is possible.

In the present work, we have developed universal model specially aimed at numerical calculation of generation process in advanced pulse-periodic high-peakpower picosecond lasers. The model describes pulse formation governed with active and passive mode locking, negative feedback, adjustable loss level in the resonator, and also taking into account the pulse profile modifying due to amplification.

Verification of the model was carried out by comparing the numerical calculation results with analytical solutions possible in extreme cases of purely active or purely passive mode locking, as well as with the results of measurements of real laser system parameters. As a result of the comparison, we can conclude the adequacy of the developed model.

Statistical analysis of calculation results allows estimating the minimum value of output pulses optical jitter attributed to the noise nature of the laser generation occurrence. As a radical measure

to reduce the magnitude of the optical jitter we propose injection of stable seed radiation in the resonator. Numerical simulations show that a significant jitter minimization is possible when injected radiation intensity two to three orders of magnitude exceeds luminescence intensity in the active element. Corresponding laser scheme is under development.

[1] M.V.Gorbunkov, A.V.Konyashkin, P.V.Kostryukov, V.B.Morozov, A.N.Olenin, V.A.Rusov, L.S.Telegin, V.G.Tunkin, Yu.V.Shabalin, D.V.Yakovlev. Pulsed-diodepumped, all-solid-state, electro-optically controlled picosecond Nd:YAG lasers. Quantum Electron., 35 (1), 2-6 (2005)

[2] Q.K.Ai, M.Chen, Y.Xu, L.Chang, L.Y.Chen, G.Li, J.H.Yang, and Y.F.Ma. Picosecond Nd:YLF Five-Passes Laser Amplifier with 20 mJ Pulse Energy. Las. Phys. 22(7), 1169–1172 (2012).

[3] A.A.Karnaukhov, V.B.Morozov, A.N.Olenin and D.V.Yakovlev. Precise synchronization of qcw pumped active-passive mode locked picosecond lasers. J. Phys.: Conf. Ser. 414, 012027 (2013).

[4] H.A.Haus. Mode-locking of lasers. IEEE J. Sel. Top. Quant. Electr., 6(6), (2000).

MONTE CARLO SIMULATIONS OF OPTICAL BRAIN IMAGING: APPROACHES, VERIFICATIONS, APPLICATIONS

Mikhail Kirillin[1,2], Anton Gorshkov[1,2], Ekaterina Sergeeva[1], Heidrun Wabnitz[3], Alexander Bykov[4], Alexey Popov[4], Teemu Myllylä[4], Vesa Kiviniemi[5]

[1]Institute of Applied Physics of RAS, 603950 Ulyanov St., 46, Nizhny Novgorod, Russia

[2]N.I. Lobachevsky State University of Nizhny Novgorod, 603000 Gagarin St., 23,

Nizhny Novgorod, Russia

[3]Physikalisch-Technische Bundesanstalt (PTB), Abbestr. 2-12, 10587 Berlin, Germany

[4]Optoelectronics and Measurement Techniques Laboratory, University of Oulu, 90570

Oulu, Finland

[5]Department of Diagnostic Radiology, Oulu University Hospital, 90570 Oulu, Finland

mkirillin@yandex.ru

Near-infrared spectroscopy (NIRS) is an actively emerging non-invasive functional diagnostic technique which found its place in functional brain imaging as a valuable tool that complements electroencephalography (EEG) and functional magnetic resonance imaging (fMRI). NIRS of the brain employs the significantly different absorption spectra of oxy- and deoxyhemoglobin allowing monitoring of the local oxygenation level within the brain and monitoring of brain activity. However, one of the main drawbacks of the NIRS technique is that the determination of the measurement volume for a given configuration is not straight-forward. In order to accurately determine it one should accurately assess the propagation of probing light within the human head taking into account the real anatomic geometry and corresponding inhomogeneities in optical properties. Possible solutions for deriving the probing radiation distribution within the human head include theoretical approaches and numerical techniques. However, the essential limitation of the theoretical approaches is that analytical solution can be obtained only for quite simple geometries for a limited number of compartments with different optical properties. This is suitable for phantom measurements; however, for assessment of in vivo measurements numerical techniques are preferable. The most common approach to numerical simulation of light transport in human head which is widely used in NIRS is the finite-difference approach to the solution of the diffuse equation, as implemented in the NIRFAST tool [1]. However, this approach does not allow for accurately calculating the distribution of radiation close to the surface and in weakly scattering regions. In this respect the Monte Carlo simulation of light transport in complex geometries appears to be a suitable solution for aims of NIRS of the brain. The main principle of this technique is simulation of a large number of random photon trajectories within tissue and further statistical analysis of the obtained results. Common approaches to account for complex geometry in Monte Carlo simulation of light transport include voxelization of the considered medium [2] or accurate description of boundaries within tissue [3, 4]. However, the first approach may lead to incorrect assessment of photon refraction at boundaries, especially in the case of cubic voxels.

In this paper we report on the development of novel Monte Carlo code for simulation of light transport in complex geometry media. The code is optimized for execution at computer systems

with parallel architecture including clusters, multicore processors, GPUs and Intel Many Integrated Core architecture. Parallelization allowed achieving up to 11-fold speed compared to single thread version. In order to further increase computational efficiency of the developed code we introduced a biasing technique allowing to significantly improve the calculation speed for a particular detector. The technique is based on possibility of substitution of current photon direction with a new one, which results in higher probability of reaching the detector, with corresponding correction of a photon weight. In order to verify the developed code we compared results of calculation of a NIRS system at three wavelengths with results of an analytical solution derived from diffusion theory. The results demonstrate good agreement. Further verification included comparison of simulation results with experimental measurements obtained from human-head-mimicking multilayer phantoms [5].

The main advantage of Monte Carlo simulations against NIRFAST is that they allow for tracing individual photon trajectories and thus accurately defining the measurement volume of a NIRS system. Additionally it allows for analysis of dependence of differential pathlength factor (DPF) on source detector separation and optical properties. DPF is widely employed when processing NIRS experimental data and usually is considered as a constant, however, numerical simulations show strong dependence on source-detector separation. Another possibility provided by Monte Carlo simulations is the separation between photons that reached grey and white matter and those which did not reach these deep tissues with respect to their contribution to the shape of the timedependent NIRS signal (classes I and II, respectively), which cannot directly be obtained from experiment. The common approach includes binary classification of the photons contributing to the NIRS signal [6]. However, such classification does not differentiate photons depending on their pathlength travelled within the volume of interest. In this respect we introduced a new photon classification where a weight of a contributing photon was divided between two classes in accordance with its pathlength within the compartments of interest (grey and white matter layers)

$$P_I = P \frac{l_{wgw}}{l_{total}}, P_{II} = P - P_I$$

where PI and PII are corresponding contributions to classes I and II, P is the weight of a photon at the detector, lwgm is a photon pathlength within grey and white matter areas and ltotal is the total photon pathlength. Such classification allowed for more relevant analysis of NIRS signal time course.

[1] H. Dehghani, M. E. Eames, P. K. Yalavarthy, et al, Commun. Numer. Methods Eng. 25(6), 711-732 (2009).
[2] Q. Q. Fang and D. A. Boas, Opt. Express 17(22), 20178-20190 (2009)
[3] H. Li, J. Tian, F. Zhu, et al, Acad. Radiol. 11(9), 1029-1038 (2004).
[4] A.V. Gorshkov and M.Yu. Kirillin, Journal of Computational Science 3(6), 498-503 (2012).
[5] V.O. Korhonen, T.S. Myllylä, M.Yu. Kirillin, et al IEEE J. Sel. Top. Quantum Electron. 20(2), 7100310 (2014).
[6] C. C. Chuang, Y. T. Lee, C. M. Chen, et al, Biomed Eng Online 11, 21 (2012).

DEEP UV LEDS EXPAND PHOTONICS WORLD: DEVICES, APPLICATIONS AND MARKETS

Sergey Paltsev[1], Yuri Bilenko[2]

[1]*Profina Oy, Finland ,Sensor Electronic Technology, Inc. (SETi),*

[2]*Columbia, South Carolina, USA.*

Deep ultraviolet light emitting diodes (DUV LEDs) with 230-360 nm wavelength, in a recent decade became a mature product for scientific and consumer markets with widening possibilities and great potential.

Sensor Electronic Technology, Inc. (SETi) has pioneered these devices and systems on its basis a decade ago, established registered trademarks of AlGaN material technology MEMOCVD and lines of products UVTOP and UVCLEAN.

Now SETi is a leading world producer of Deep UltraViolet LEDs and systems.

This new light source has many critical advantages:compared to existing light source (Mercury, Deuterium, Xenon lamps) of this UV waveband

- Optimum application wavelength (s) with instant on/off;

- Mechanically robust and compact, flexible design;

- Low voltage and promising WP efficiency.

This features are beneficial in analytical instrumentation market, as spectroscopy, chemical analysis. sensors, bio- and medical research, phototherapy, curing, and in UV-disinfection, and also in creating new applications (fruit storage, electrical charge management).

Current developed applications include quantitative measurement of critically important chemical and bio-substances - proteins, chemical agent, fluorescent and biomarkers. Interesting application lies in a field of UVB interaction with living substances (vitamin D formation, prolongation of berries and fruits shelf life and many other application).

Phototherapy with UV-B LED has been FDA approved a tremendous perspectives.

The main mass market will be water and surface sterilisation due to fact what 250-280 nm light is very active in DNA/RNA of bacteria and viruses destruction. This technology is NASA, ISO and AS9100 certified and has been successfully used since February 2014 in International Space Station Microgravity Glove Box decontamination

FIDIPRO PROJECT ON BIOPHOTONICS: FINLAND-RUSSIAN COLLABORATION

Valery V. Tuchin

Research-Educational Institute of Optics and Biophotonics, Saratov State University, Saratov 410012, Russia

Laboratory of Laser Diagnostics of Technical and Living Systems, Institute of Precise Mechanics and Control RAS, Saratov, 410028, Russia

Interdisciplinary Laboratory of Biophotonics, Tomsk State University, Tomsk 634050, Russia

The project "Biophotonics technologies for novel diagnostic and therapeutic applications" has been funded by TEKES Finnish Distinguished Professor (FiDiPro) -program to work in Finland during 6/2011 – 8/2014.

The focus of the project was to study the tissue optical clearing (OC) for improving capability of the optical techniques and devices to be used for non-invasive diagnostic and therapeutic treatment of tissues [1]. The OC studies were performed both on phantoms and on tissue samples. Skin, fat, muscle, skull, brain, cartilage, and some others were used as tissue models.

Phantoms having similar optical properties as real tissues were designed, fabricated and tested. Monte Carlo simulations were carried out to model light propagation in different multilayered tissues such as skin and brain. Testing of some OCAs was performed on designed phantoms with real capillary structure and on tissues in vitro. In addition, effect of OC on elastic light scattering at a single cell level was demonstrated [2].

An optical imaging technology capable for imaging at depths of 1 cm or larger, which uses upconversion luminescent nanoparticles as a contrasting agent and tissue OC was designed. Outstanding performance was based on the particles ability to absorb and emit light in the spectral region, least affected by tissue scattering and absorption at application of an OCA.

Along with this, a near-infrared spectroscopy system was tested and improved. This system was used to verify our mathematical model and phantom for brain and skull. A further aim is to use the system simultaneously with magnetic resonance imaging system, which sets certain limitations on the design.

This project was devoted only to some aspects of light-tissue interactions, being focused on light scattering by tissues and tissue models. The proposed methods and presented results allow us to make certain conclusions and predictions concerning the directions of further investigations in the field of tissue optics and nanophotonics and the development of optical diagnostic and therapeutic medical systems [1].

The designing of laser photoacoustic imaging systems can be considered as a very prospective direction in biomedical optics that allows one to provide an impressive contrast and resolution in the imaging of both deep and superficial small tumors and cancer cells in lymph nodes and blood vessels. PA technique should be optimal for the diagnosis of tissues at the middle depths, where time-resolved diffusion, OCT, and multiphoton methods are not effective. This opens up applications in whole body imaging, brain function, oxygen saturation, label-free cell analysis, and noninvasive cancer biopsies including evaluating sentinel lymph nodes for breast cancer staging. As it was proved recently optical clearing may significantly help is solution of this

ambitious problem.

Currently, investigation of superficial tissue layers with the use of OCT can provide important results and offer much promise for medical applications, especially for ophthalmology, early cancer detection of skin and the cervix, blood microcirculation analysis, and the endoscopic/ laparascopic/needle-based studies of blood vessel wall, mucous of internal organs, breast, muscle, cartilage, lung and many other tissues and organs. The FiDiPro project also gives some input in this global problem mostly due to designing of OC technologies.

The immersion OC technique allows one to effectively control the optical properties of tissues and blood. It has great potentiality for noninvasive medical diagnostics using confocal microscopy, OCT, two-photon excitation fluorescence (TPEF), second harmonic generation (SHG), phase-resolved and speckle techniques, due to the rather small thickness of tissue layers usually examined by these methods, which allows for fast impregnation of a target tissue at a topical application of an immersion agent.

Figures 1 and 2 illustrate OC assessment of deep cartilage layers and cartilage-bone interface by using a commercially available OCT system (Thorlabs Inc., 930 nm). The solution of Iohexol (OmnipaqueTM) in water has been used as an OCA. The cartilage-bone boundary becomes visible after 15 min of OC that enabling non-invasive estimation of its roughness: $Sa = 10\pm1\mu m$.
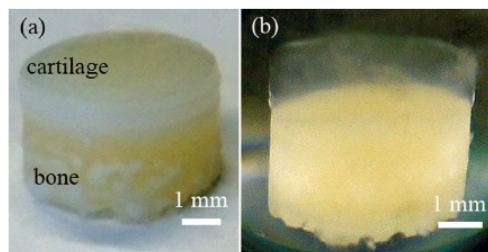
Fig. 1. The osteochondral samples: natural appearance of the sample before (a) and after OC by Iohexol (OmnipaqueTM) solution has been completed (b) [3].
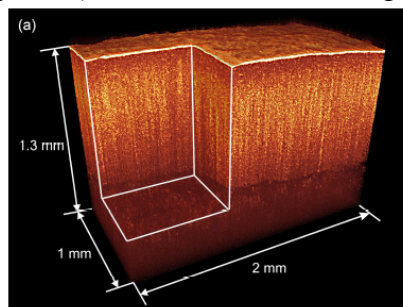
Fig. 2. 3D OCT image of the cartilage after 15 min of OC by Iohexol (OmnipaqueTM) solution. The extracted from OCT data average roughness of the cartilage-bone interface $Sa = 10 \mu m$ [3].

[1] V.V. Tuchin, Tissue Optics: Light Scattering Methods and Instruments for Medical Diagnosis, 3rd ed. ((SPIE Press, Bellingham, WA, 2015).
[2] M. Kinnunen, A. Bykov, J. Tuorila, T. Haapalainen, A. Karmenyan, and V. Tuchin, J. Biomed. Opt.19 (7), 071409 (2014).
[3] A. Bykov, T. Hautala, M. Kinnunen, A. Popov, S. Karhula, S. Saarakkala, M.T. Nieminen, V. Tuchin, and I. Meglinski, J. Biophoton. (2015), doi: 10.1002/jbio.201500130.

LASER-INDUCED SEMICONDUCTOR NANO- MICROSTRUCTURES WITH CONTROLLED TOPOLOGY: FUNCTIONAL PROPERTIES AND VERIFICATION OF MACROSCOPIC QUANTUM EFFECTS IN THIN-FILM AND CLUSTER SYSTEMS

A.Antipov[1], S.Arakelian[1], A.Kucherik[1], S.Kutrovskaya[1], D.Nogtev[1], A. Osipov[1], T.Vartanyan[2], S.Zimin[3]

[1]Vladimir State University named after A.G. and N.G. Stoletovs, Vladimir, 600000, Russia

[2]St. Petersburg National Research University of Information Technologies, Mechanics and Optics, St. Petersburg, 197101 Russia

[3]P. G. Demidov Yaroslavl State University, Yaroslavl, 150000, Russia

e-mail: arak@vlsu.ru

1. The paper represents the results of laser synthesis of nanoparticles/semiconductor nanoparticles by methods of both laser modification of thin films and laser evaporation of substance in liquid to produce the colloidal systems. The analysis of induced nanostructures has been carried out by absorption spectroscopy, scanning electron microscopy and transmission electron microscopy. Laser-induced surface and thin films nanostructures with controlled topology result in variation of morphological and optical characteristics of induced nanostructures. Under a laser radiation impact, the nanoparticles become quantum dots. The bimodal size nanoparticle distribution occurs, and analysis can be carried out in analogy with quantum kinetic processes. By colloidal droplet deposition technique, the nanostructures with various morphology (vs the substrate temperature) has been fabricated.

2. By a cw-laser ablation experiment (λ=1.06μ, laser intensity – up to 10^6W/cm^2) with colloidal systems, induced surface semiconductor PbTe nanostructures on solid substrate have been used to study the electrical transport properties under quantum tunneling effect and/or jump conductivity (in the frames of a shell model cluster approach), i.e. the macroscopic quantum phenomena development vs cluster size a and distance d between neighboring units. Comparison of sizes a of the particles being obtained with the value of exciton Bohr radius a_B shows that the strict condition $a \leq a_B$ = 50-100 nm is true. The above comparison enables to say that the conditions of dimensional quantization are satisfied for PbTe nanoparticles. On the other hand, when the nanoparticles drop on the solid surface they are accumulated in clusters of bigger size. So, we can study the macroscopic quantum phenomena development in dependence on a. The island conductivity is dominant for the case. An electroresistance can dramatically decrease due to spontaneous selected multichannel/parallel electron transportation trajectories. Two conditions are the vital items for that: (i) cluster size $a<\ell$, where ℓ is the inelastic length for charged nanoparticles/electrons, and (ii) distance d between two neighboring clusters less the de Broglie wavelength λ_{dB}: d « λ_{dB} .

3. In progress, we should carried out the more detailed study of the correlation between the nanostructure topology and functional dynamic properties and also, optical characteristics (including a quantum domain) of the unit. The solution of the existing problems will allow us to respond to modern challenges for the creation of new hybrid (optics/photonics + electronics) technologies for fast femtophotonics/microelectronics – by synthesis of nano- microstructures on the surface of various materials.

APPLICATION OF ATOMIC LAYER DEPOSITION IN POLYMER BASED NANOPHOTONIC DEVICES

Seppo Honkanen[1], Markku Kuittinen[1], Jyrki Saarinen[1], Matthieu Roussey[1], Rizwan Saleem[2], Petri Stenberg[1], Leila Ahmadi[1], and Rizwan Ali[1]

[1]Institute of Photonics, University of Eastern Finland, P.O. Box 111, Joensuu, Finland

[2]National University of Sciences and Technology (NUST), Islamabad, Pakistan

seppo.honkanen@uef.fi

Polymers are materials that have a great potential for fabrication of low-cost photonic devices. The possibility of fabricating polymeric structures by using replication methods, such as nanoimprint lithography, enables cost efficient large scale manufacturing, which is often required for commercial products. Good examples of such products are (disposable) lab-on-a-chip (LOC) sensors [1]. The application of Atomic Layer Deposition (ALD) in connection with the replicated polymeric devices can greatly increase the functionality of these devices. ALD is a unique thin film deposition method based on saturative surface reactions of alternately supplied precursor vapors [2]. Due to the saturation of each reaction step, the film growth is self-limiting, thereby providing several unparalleled advantages: i) atomic level control of film composition and thickness, ii) perfect step coverage, and iii) large-area uniformity. In addition, ALD is highly suitable for large-scale manufacturing. As in the fabrication of plastic nanophotonic devices, even the low-cost roll-to-roll method can be employed in the ALD process. In our approach, we combine the replication techniques with ALD, which can lead to ultra-low-cost polymer-based nanophotonic devices for a variety of applications.

Here we summarize our recent results on using ALD in combination with a variety of polymer-based nanophotonic devices. The nanostructures are first fabricated in polymer substrates using nanoimprint lithography. The nanoimprinting process is followed by depositing amorphous TiO2 or TiO2/Al2O3 bilayers on top of the polymer structures. The studied nanophotonics devices include a guided-wave Young's interferometer and guided-mode resonance filters (GMRFs). Examples of these hybrid organic/inorganic structures are shown figure 1.
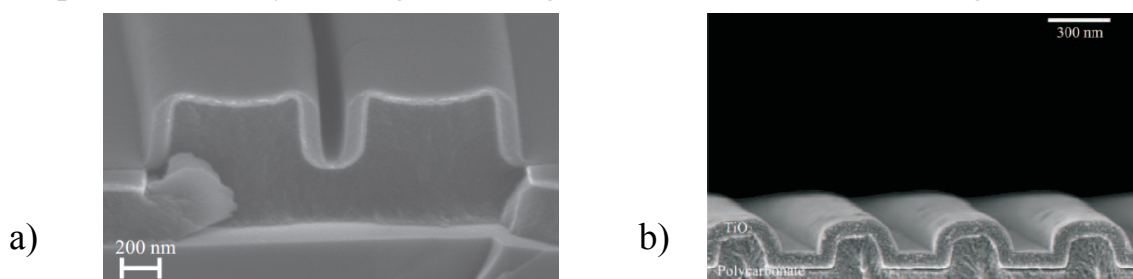
Fig. 1. SEM image of a cross section of a) an ALD-coated polymeric slot waveguide and b) an ALD-coated polymeric guided-mode resonance filter (GMRF).

[1] C. D. Chin, V. Linder, and S. K. Sia, Lab Chip 7, 41-57 (2007).
[2] M. Ritala and M. Leskelä, in Handbook of Thin Film Materials, H. S. Nalwa, Ed., (Academic Press, 2001), p. 103.

SIMULTANEOUS GENERATION OF X-RAY AND TERAHERTZ RADIATION PRODUCED BY INTENSE FEMTOSECOND LASER PULSES FROM ATOMIC CLUSTER PLASMA

Alexander Shkurinov

Lomonosov Moscow State University, Moscow, 119992 Russia

ashkurinov@physics.msu.ru

Abstract — The present paper analyses the main mechanisms and properties of terahertz radiation generated by intense femtosecond laser pulses from gas and nanosize gas clusters. The possibilities of simultaneous generation terahertz and x-ray radiation are discussed and demonstrated experimentally.

The present paper demonstrates the possibility of simultaneous generation of X-ray and THz radiation in a gas cluster jet by intense femtosecond laser pulses. We present the concept of developing of "X-ray-optical-THz" sources of ultrashort pulse duration. We demonstrated that optimal conditions for THz and characteristic X-ray radiation in gas-cluster jets are different. This allows to control the ratio of values and the relative temporal delays of simultaneously generated signals at THz and X-ray frequencies by means of changing the temporal delay between laser pulses and the moment of cluster stream formation, and also when changing chirp parameters of the exciting laser pulses. The diagram showing the direction of the generated THz radiation in the near-axial area represents the cone with semiapex angle of 3.7 degrees and the minimal value in the near-axial area of the beam. The angular area less than 15 degrees was studied.

The THz radiation, generated in the laser-induced cluster plasma excited by linearly polarized optical radiation is also linearly polarized. The dependence of THz signal value on excessive gas pressure, which creates a stream, in the dichromatic system has a nonlinear character and the THz radiation, generated in the laser-induced cluster plasma excited by linearly polarized optical radiation is also linearly polarized. The dependence of THz signal value on excessive gas pressure, which creates a stream, in the dichromatic system has a nonlinear character and demonstrates saturation in high pressure. The absence of saturation of the volume of THz radiation signal with the growth of energy of exciting pulses at the main frequency observed up to 25 mJ in the pulse, agrees with the published earlier data for both monochromatic and dichromatic systems of optical excitation, and in our experiments up to 80-100 mJ saturation doesn't take place either. Absence of saturation will allow in perspective get THz pulses of higher energy by means of increasing the energies of exciting optical pulses. The comparative analysis of the obtained experimental data showed that given equal average atom concentrations, THz radiation generation in static gas takes place with a higher optical-THz conversion coefficient than in gas-cluster streams. This effect can be connected with a relatively small volume of plasma waist and accordingly, with a considerably smaller number of atoms/molecules taking part in the interaction in the latter case.

The influence of laser plasma transparency on the THz frequency is also discussed. It has been demonstrated that argon clustering leads to the power decrease of THz signal in the near-axial area in the case of dichromatic pumping. One of the possible explanations is the formation of hyper critical cluster plasma. It has been demonstrated experimentally that by means of through changing the ratio of buffer and cluster gases in the gas mixture one can effectively change the

value of THz radiation generated in the cluster stream. In the carried out experiments the highest efficiency of THz radiation generation was observed when the gas mixture of Ar (argon) + He (helium) was used with the 1:10 ratio. It seems productive to carry on research in this direction and proceed in the future to mixed clusters, formed at supersonic discharge from the nozzle of double, triple mixtures of multiatomic molecules with inert gases. For the purpose of correct interpretation of the experimental data a model was made which took into consideration the frequency of the cluster own oscillation in the shape of an ellipse. A hypothesis was suggested that widening the resonance in THz radiation observed in a number of experiments of other research groups is connected with the spread in sizes and shapes of clusters. The power of dipole and quadrapole cluster radiation at THz range frequency is the result of action of ponderomotive Miller force and the power of radiation pressure. It has been established that the calculated dependence of the power of THz radiation on the power of laser radiation agrees with the experimental results.
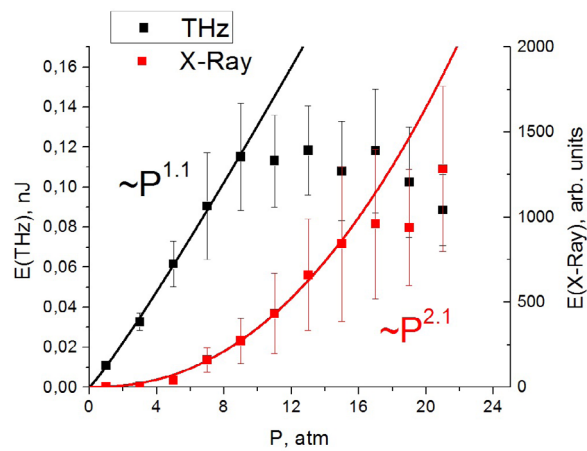
Fig. 1. Terahertz and X-ray radiation versus the argon gas cluster pressure

EXPERIENCE IN COLLABORATIVE CONSTRUCTION AND BIOMEDICAL APPLICATIONS OF LASER TWEEZERS

Priezzhev A.[1,2], Lee K.[1,3], Kinnunen M.[3], Myllyla R.[3], and Meglinski I.[3]

[1]Laser Biomedical Photonics Laboratory, Physics Department, [2]Intertational Laser Centre, Lomonosov Moscow State University, Moscow, Russia, [3]Optoelectronics and Measurement Techniques Laboratory, University of Oulu, Oulu, Finland

avpriezz@gmail.com

Laser tweezers (LT), also referred to as optical traps (OT), is a novel technology that has emerged in the 1970-s. It opened new possibilities to handle and manipulate without any mechanical contact the microparticles of different nature and to measure molecular-level (picoNewton scale) forces of the interaction between them and with the environment. Due to extremely wide area of potential applications of this technology it gained intensive development and many research groups went into designing new schemes and operation modes of LT and exploring their new application perspectives.

Given the experience of long lasting scientific collaboration in the field of biophotonics between our laboratories, we decided to jointly enter this field of research and build two similar LT set-ups in Oulu and in Moscow for biophotonics applications. The initially set problem was to study the peculiarities of light scattering by non-spherical red blood cells (RBC) and their aggregates, and the biophysical mechanisms behind RBC interaction in the process of reversible aggregation. Measurements with the LT were backed with digital calculations of light scattering effects from nonspherical particles and extensive studies of RBC microrheology with other optical techniques, in particular, laser backscattering aggregometry (LBA) from whole blood samples, which we had been also developing for a number of years. In comparison with LT-assisted single cells level measurements, LBA yielded data averaged over millions of cells, this approach having its advantages and limitations. It is of fundamental interest to compare the information about the RBC interactions that can be obtained with LT and LBA. Implementation of these techniques into clinical practice has a perspective of drastic improvements in the health-care of patients suffering from cardio-vascular and various systemic diseases, like diabetes.

The OT are formed with orthogonally polarized cw laser beams from two single mode diode pumped Nd:YAG lasers with the output power up to 250 mW. Large numerical aperture water immersion objective is used to tightly focus the laser beams and form two OT. The RBC trapping force can be varied in the range from 1 to 20 pN. Visual control of the trapped cells is implemented with a CMOS camera.

We will present the latest results obtained with our LT devices including the measured RBC light scattering phase functions and the measured dependencies of the cells interaction forces on the content of the environmental medium. The presentation will be assisted with the real time video recordings of the cells interaction processes.

QUANTIFIED MONITORING OF SKIN OCT-IMAGE EVOLUTION UNDER EXTERNAL ACTION

P.D. Agrba[1,2], M.A. Pasukhin[1], and M.Yu. Kirillin[2,1]

[1]Lobachevsky State University of Nizhny Novgorod

[2]Institute of Applied Physics of Russian Academy of Sciences

agrbapd@gmail.com

Introduction. Optical coherence tomography (OCT) is a modern technique of visualization of internal structure of biotissues at the depth up to several mm with resolution down to several μm [1-3] based on low coherence interferometry that employs information from photons backscattered from inhomogeneities of refractive index within the biotissue. However, evaluation of tissue conditions based on qualitative analysis of OCT-images depends on external conditions (compression, temperature regime) and clinician subjectivism, which deteriorates diagnostic value of OCT. In order to enhance this value it is preferable to use impersonal method for OCT-image assessment. Such methods allow obtaining additional information about biotissue that could be taken into account in a line with qualitative information. In this work we used the histogram of an OCT-image for quantitative assessment of biotissue condition. The aim of this work was to compare histograms of OCT-images of normal human skin with those of skin under external action (mechanical compression, extreme temperature regimes) or with pathology (psoriasis, scleroderma) in the course of medical treatment.

Materials and methods. The study was performed in vivo on human volunteers. At the first stage of work we studied alterations of histogram of skin OCT-image under longterm pressure (several minutes) and after preliminary temperature action (heating or cooling). The pressure to the inspected skin area was kept equal to 0.21 N/mm2. OCT images of skin were obtained each 5 seconds after measurement start during 7 minutes. At the second stage we performed the study of histogram assessment in OCT skin monitoring in course of therapy of such skin pathologies as psoriasis and scleroderma. The OCT-images for each patient were obtained before therapy start, in the middle of therapy period and at the end of therapy period. Each time three OCT-images with constant pressure were obtained: immediately after measurement start, in 30 second, and in 1 minute. This approach allowed comparing histograms without and with compression effect. In course of the assessment an OCT-image was divided into fragments containing only noise signal and the one combining useful signal with noise (Fig. 1a). For each fragment the histogram was calculated. The histogram of the noise fragment was further used to separate noise component from the histogram of fragment containing useful image (Fig. 1b). The resultant histogram was approximated by an analytical function represented by a sum of two exponentials with three parameters (width, height, shift) for each of them:

$$S = a_1 \cdot e^{-\left(\frac{b_1-x}{c_1}\right)^2} + a_2 \cdot e^{-\left(\frac{b_2-x}{c_2}\right)^2} \tag{1}$$

Alterations of these parameters were treated as impersonal criteria of alterations of biotissue condition.
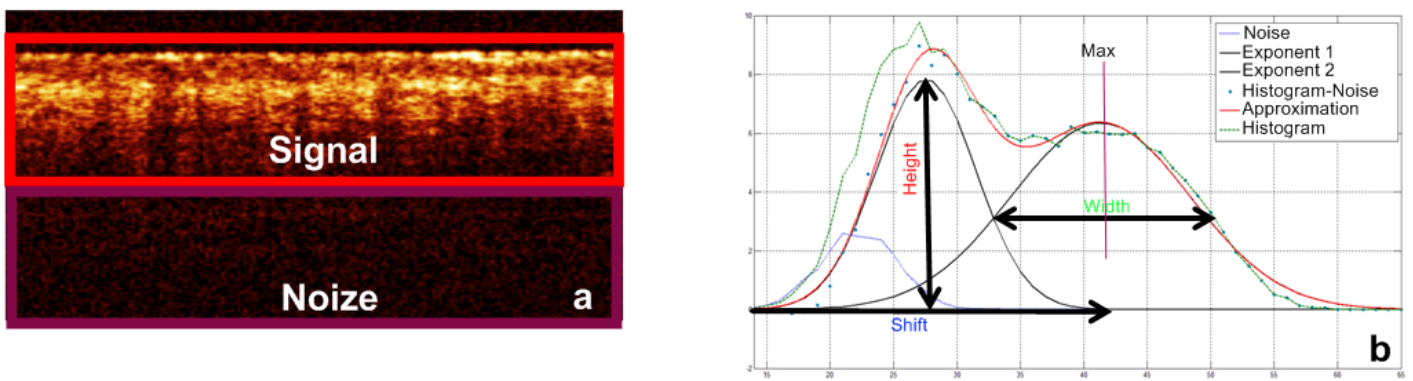
Fig. 1. OCT-image separated into fragments containing only noise signal and the one combining useful signal with noise (a) and process of histogram calculation (b).

Results and discussion. The algorithm of OCT-image histogram analysis was firstly approbated in OCT monitoring of effects of compression, cooling or heating on human skin in vivo. We demonstrated that all the considered parameters are sensitive to changes in OCT images induced by these external actions. In particular, parameter a_1 increased under mechanical compression and during skin relaxation after preliminary heating and weakly decreased after preliminary cooling. Parameter a_2 increased after preliminary heating and decreased for other considered actions cases. Parameter b_1 was not affected by compression and grew weakly after thermal action. Parameters b_2 and c_2 demonstrated similar increase in all cases. Parameter c_1 increased after preliminary heating and slightly alternated for other cases.

The second stage of the study included OCT image analysis in course of OCT monitoring of psoriasis and scleroderma treatment. It was shown that changes in OCTimages caused by therapy followed by changes of histogram parameters of respective OCT-images. Thereby employment of histogram analysis can potentially serve for quantification of changes in pathologic skin induced by therapy, however, further studies are required to statistically prove our assumptions and choose proper parameters mostly affected by corresponding changes in inspected skin. It should be noted that at the end of treatment parameters may differ from those for norm, because healing can last after the end of treatment. Nevertheless, proposed parameters can be used as additional information about skin condition and potentially can increase diagnostic value of the OCT technique.

[1] B. E. Bouma and G. J. Tearney – eds., Handbook of Optical Coherence Tomography, (Marcel Dekker, New York, 2002)
[2] V.M. Gelikonov, G.V. Gelikonov, L.S. Dolin, V.A. Kamensky, A.M. Sergeev, N.M. Shakhova, N.D. Gladkova, E.V. Zagaynova, Laser Physics, 13(5), 692-702 (2003).
[3] A.M. Sergeev, L.S. Dolin, D.N. Reitze, Optics & Photonics News, 28-35 (2001

EFFECTS OF CISPLATIN ON THE LEVEL OF HYDROGEN PEROXIDE AND CELL DEATH IN HELA KYOTO CELLS

A.S. Belova[1,2], A.G. Orlova[1,2,3], I.V. Balalaeva[2], N.N. Razumkova[2], A.V. Maslennikova[1,3], N.M. Mishina[3,4], N.M. Shakhova[1,3], E.V. Zagaynova[3],V.V. Belousov[3,4]

[1]*Institute of Applied Physics of the Russian Academy of Sciences, Nizhny Novgorod,*

Russia

[2]*Lobachevsky State University of Nizhny Novgorod, Nizhny Novgorod, Russia,*

[3]*N. Novgorod State Medical Academy, Nizhny Novgorod, Russia*

[4]*Shemyakin-Ovchinnikov Institute of Bioorganic Chemistry, Moscow, Russia*

Chemotherapy is one of the main techniques for treatment of malignant tumors. Hydrogen peroxide (H2O2) was supposed to play a key role in carcinogenesis [1]. It was assumed that in normal cells reactive oxygen species (ROS) originating from NADPH oxidase are at low levels, and the concentration of H_2O_2 is regulated by the glutathione system; while in tumor cells high levels of ROS close to the threshold of cytotoxicity are produced through the mitochondrial respiratory chain, and H_2O_2 concentration is controlled by catalase [2]. Several studies demonstrated that cancer cells are more susceptible to H_2O_2-induced cell death than normal cells [3-4]. The aim of our study was the investigation of the level of hydrogen peroxide and mechanisms of cell death in tumor cells in vitro after exposing them with cisplatin.

Materials and methods

Cell line of human cervical carcinoma HeLa Kyoto expressing the cytosolic sensors was used. Two types of sensors, HyPer2 and HyPer2-C199S, were used in our experiments. HyPer2 is the sensor of hydrogen peroxide, however, it is also sensitive to changes in pH level. HyPer2-C199S is sensitive only to changes in pH level. There were several concentrations of cisplatin in our experiments: control (0.0 µg/ml),1/2 × IC50 (1.25 µg/ml), IC50 (2.5 µg/ml), 2 × IC50 (5.0 µg/ml), 4 × IC50 (10.0 µg/ml), 10 × IC50 (25 µg/ml), and 60 µg/ml. IC50 is the concentration of cisplatin causing loss of viability in 50% of cells. The exposure times were 6, 12, and 24 hours. Flow cytometry with markers for apoptosis and vital dye (PE-Annexin V and 7-AAD) was employed for monitoring of cells response. Sensors reaction was registered in the same cells in parallel.

Results

We demonstrated the absence of differences in mechanisms of cell death between HeLa Kyoto-HyPer2-C199S and HeLa Kyoto-HyPer2. Increase in percentage of early apoptotic cells after 12 hours of incubation with cisplatin in concentrations of 10.0 µg/ml and higher and after 24 hours incubation with cisplatin in concentrations of 5.0 µg/ml and higher was observed.There was no difference in fluorescence intensity of both sensors after 6 hours of incubation with all considered concentrations of cisplatin. Increase in fluorescence intensity of HyPer2 with increase of cisplatin concentrations after 6 hours of incubation was detected. However, HyPer2-C199S did not demonstrate any significant variation of fluorescence intensity in these conditions. The difference in reactions of sensors after 24 hours of incubation with cisplatin is more pronounced. These changes were typical for living cells and early apoptotic cells, but not for dead cells. Examples of sensors reaction to cisplatin are shown in Figure 1.

H$_2$O$_2$ sensitive sensor   H$_2$O$_2$ insensitive sensor
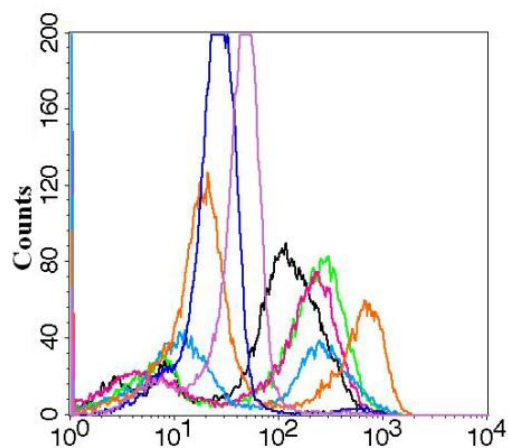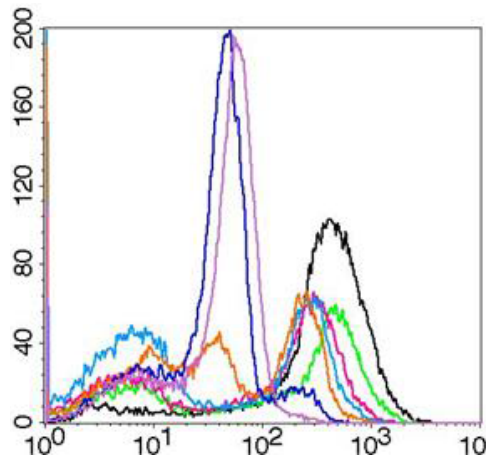
HyPer2 fluorescence intensity, a.u.   HyPer2-C199S fluorescence intensity, a.u.

Fig.1. Representative histograms of HyPer2 fluorescence (left) and HyPer2-C199S fluorescence (right) after 24 hours of incubation with cisplatin in different concentrations. Red arrow indicates HyPer2 reaction.

Conclusion

Increasing fluorescence of HyPer2 with the background of almost constant level of HyPer2-C199S fluorescence allows suggesting that increase in the cisplatin concentration leads to an increase in the amount of hydrogen peroxide. Taking into account that HyPer2 reaction was observed only for viable and early apoptotic cells, the detected response was not a consequence of cell death.

[1] Lopez-Lazaro M, Cancers Letters, 252, 1-8 (2007).
[2] C. Nicco, A. Laurent, C. Chereau, B. Weill, F. Batteux, Biomed. Pharmacother, 59, 169–174 (2005).
[3] H. Maeda, S. Hori, H. Ohizumi, T. Segawa, Y. Kakehi, O.Ogawa, A. Kakizuka, Cell Death Differ, 11, 737– 746 (2004).
[4] Q. Chen, M.G. Espey, M.C. Krishna, J.B. Mitchell, C.P. Corpe, G.R. Buettner, et al., Proc. Natl. Acad. Sci. USA, 102, 13604–13609 (2005).

SUPERFILAMENTATION IN WATER WITH TIGHT FOCUSING LASER BEAMS: FROM FEMTOSECONDS TO MICROSECONDS

F. V. Potemkin, E. I. Mareev, A. A. Podshivalov, V. M. Gordienko

Faculty of Physics and International Laser Center M.V. Lomonosov Moscow State University, Leninskie Gory, bld.1/62, 119991, Moscow, Russia

potemkin@automationlabs.ru

Abstract: We report whole life cycle of superfilament excited in tight focusing beams in water. Extreme energy delivery achieved under superfilamention is reflected in strong post-effects (cavitation bubbles and shock waves), which can completely characterize superfilament. OCIS codes: (260.5950) Self-focusing; (190.7110) Ultrafast nonlinear optics; (110.5125) Photoacoustics

When the ultrashort laser beam with a peak power much above critical power of self-focusing propagates through the nonlinear medium the filament can be fired. Usually filamentation is defined as a self-channeling of laser radiation due to a dynamical balance between Kerr self-focusing, plasma defocusing and diffraction. The generated electron density has a threshold like response to the energy increase, which saturates self-focusing locally and limits the peak intensity inside the filament by defocusing the beam. Therefore, a future increase of laser energy does not lead to the rise of laser intensity on the filament axis, instead the filament breaks into the multiple single filaments. Recently it was shown, that loose focusing of supercritical femtosecond laser pulse in air lead to formation of the superfilament – dense filament bundle which can no longer be described by binary interactions. In the work we report the first time a superfilament formation in water under tight focusing. The tight focusing of high-power femtosecond pulses clamps energy in a thin channel and the superfilament is generated [1]. The extreme intensity along the filament axis leads to the high plasma electron density (about $0.1 n_{cr}$). Due to the high temperatures ($T_e \sim 10 eV$) in the laser plasma, a thin layer of water vapor, surrounding the plasma, is formed. It begins to expand with a supersonic speed, then a shock wave separates from the layer and it forms a cavitation bubble [2,3]. Because the energy is transmitted from the plasma to the medium through electron-ion collisions, initially the cavitation bubble and the shock front shape replicates the shape of the laser-induced plasma[4]. Therefore, the laser-induced shock waves and cavitation bubbles are ideal tools for probing the electron density, and therefore intensity distribution in the medium. To observe the dynamical post-effects we used the shadow photography technique. First, we investigated the role of focusing geometry and showed that only in the case of tight focusing (NA>0.1) superfilament can be formed. Each point of the filament becomes a center of spherical shock waves and cavitation bubble formation. The overlapped shock waves form one contrast cylindrical shock wave and multiple cavitation bubbles transform into one cylindrical cavitation area. In the case of loose focusing the electron concentration (about $3 \times 10^{18} cm^{-3}$) is not high enough for shock wave launching (threshold about $10^{19} cm^{-3}$), but the cavitation bubbles (threshold about $10^{18} cm^{-3}$) can still be generated. However, they are located in the nonlinear Kerr foci, which are randomly distributed along the filament axis. Thereby, in the shadow photographs a stochastic pattern of laser induced cavitation bubbles is observed.

In the intermediate focusing regime (0.1<NA<0.3) the initially formed superfilament breaks into multiple filaments after passing about 1mm distance [5].
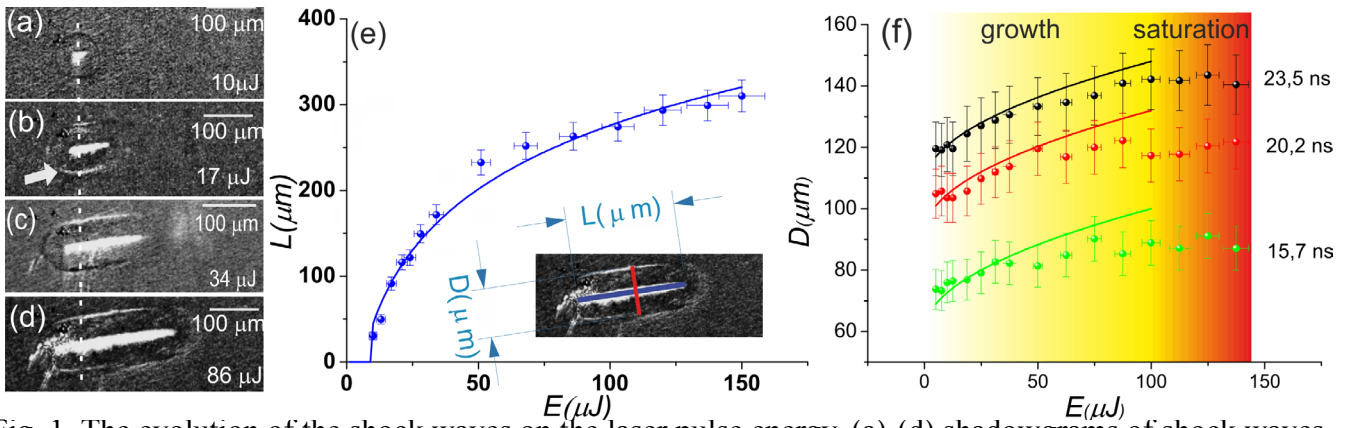
Fig. 1. The evolution of the shock waves on the laser pulse energy. (a)-(d) shadowgrams of shock waves, delayed on 18.6 ns from optical breakdown at different incident laser pulse energy: (a) 10, (b) 17, (c) 34, (d) 86μJ. The laser radiation was focused by the 3.3mm focusing lens. The bright region in the center shows plasma location. The contour outside plasma region shows laser-induced shock wave front.(e) Plasma channel length L as a function of laser energy E. Line corresponds to logarithmic dependence. (f) Shock wave diameter D as a function of laser pulse energy E. Three series of experimental data were measured at the time delays equal to 15.7, 20.2 and 23.5 ns respectively. Lines show square root dependence.

The length of the superfilament and the filament-induced shock waves logarithmically grow with the energy increase, but the diameter of the shock wave tends toward saturation as a square root of the energy. Therefore, the intensity and electron density is limited by the intensity clamping.

We for the first time investigate the superfilament and filament formation in a strongly absorbing media. Water strongly absorbed radiation on the laser wavelength due to a resonance with H_2O molecule vibrations (about $0.9cm^{-1}$); such high absorption strongly violates the processes of filament formation and further shock wave and cavitation bubble generation. Heavy water has similar physical properties to water, but it has different vibrational frequencies that allowed us to avoid resonant interaction between the laser radiation and water molecules. The most significant role the absorption of the laser energy will play is in the case of loose focusing, because the absorbed energy is exponentially depend on the distance traveled by the laser beam inside the medium. When the laser radiation was focused into a cell with D_2O, the visibility of the filament and the number and size of the cavitation bubbles (the volume of the cavitation area determines the energy delivery to the medium) was greater than in the case of H_2O. When the laser radiation is tightly focused into the water cell, the role of linear absorption is not as important, because the distance that laser radiation travels through the medium is not long enough to absorb a significant part of the energy. The experiments show that with a decrease of focusing distance, the length of the plasma channel grows.

The tight fociusing of laser radiation lead to spherical aberrations resulting from a small refractive index mismatch on the boundary. They create aberration maxima on the optical axis[6]. In these maxima multiple filaments are formed and they become a center of cavitation bubble and shock wave formation. Aberrations sufficiently complicate the evolution of the cavitation area, which lead to the jet emission at the last stage of cavitation bubble evolution. A more complicated theory of the process can be found in[6] .
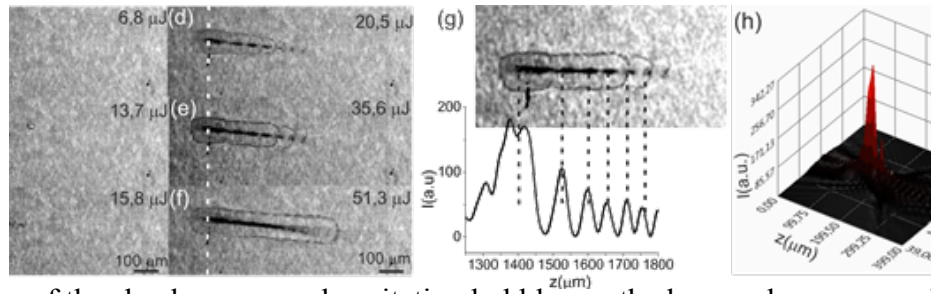
Fig. 2. The evolution of the shock waves and cavitation bubbles on the laser pulse energy with aberrations. (a)-(f) shadowgrams of shock waves and cavitation bubbles, delayed on 18.6 ns from optical breakdown at different incident laser pulse energy: (a) 6.8, (b) 13.7, (c) 15.8, (d) 20.5, (e) 35.6 and (f) 51.3 µJ. The laser radiation was focused by the 4.6mm focusing lens (NA=0.3). (g,h) The numerical calculation of the intensity profiles after focusing of the laser beam into water for NA=0.3, d=1,3mm and the shadow picture of the corresponding laser-induced shock waves and cavitation bubbles.

References

[1] Point G, Brelet Y, Houard A, Jukna V, Milián C, Carbonnel J, Liu Y, Couairon A and Mysyrowicz A 2014 Superfilamentation in Air Phys. Rev. Lett. 112 223902

[2] Potemkin F V, Mareev E I, Podshivalov a a and Gordienko V M 2014 Laser control of filament-induced shock wave in water Laser Phys. Lett. 11 106001

[3] Potemkin F V and Mareev E I 2015 Dynamics of multiple bubbles, excited by a femtosecond filament in water Laser Phys. Lett. 12 015405

[4] Lauterborn W and Vogel A 2013 Bubble Dynamics and Shock Waves ed C F Delale (Berlin, Heidelberg: Springer Berlin Heidelberg)

[5] Abraham E, Minoshima K and Matsumoto H 2000 Femtosecond laser-induced breakdown in water : time-resolved shadow imaging and two-color interferometric imaging Opt. Spectrosc. 176 441–52

[6] Marcinkevičius A., Mizeikis V, Juodkazis S, Matsuo S and Misawa H 2003 Effect of refractive index-mismatch on laser microfabrication in silica glass Appl. Phys. A Mater. Sci. Process. 76 257–60

PHOTO-INDUCED PHENOMENA IN CHALCOGENIDE GLASSES IRRADIATED BY HIGH-INTENSITY LASER PULSES

Elena A.Romanova[1], Yu.S.Kuzyutkina[1], S.Guizard[2], N.Abdel-Moneim[3], D.Furniss[3], A.B.Seddon[3], T.M.Benson[3]

[1]Saratov State University, Astrakhanskaya 83, 410012 Saratov, Russia

[2]Laboratoire des Solides Irradiés,CNRS-Ecole Polytechnique, Palaiseau, France

[3]University of Nottingham, Nottingham, UK

romanova@optics.sgu.ru

Chalcogenide glasses are non-crystalline semiconductors transparent in mid-infrared. They exhibit strong third-order non-linear optical response and high photo-sensitivity [1]. A theory of the non-linear optical response of non-crystalline semiconductors has not been yet developed because of the specific energy bands structure that does not fit a two-band model, which is used in the theory of crystalline semiconductors. Due to energy levels in a bandgap, fundamental absorption band (FAB) edge of a non-crystalline semiconductor has a spectral range of exponential decay (Urbach tail). For experimental study of the non-linear optical response of the glass compositions $As_{40}Se_{60-x}S_x$ we have used an interferometric pump-probe method [2]. When a high intensity pump pulse was focused on a glass sample shaped as thin disk at some time between probe and reference pulses, the probe pulse experienced a disturbed dielectric constant ε. The induced phase shift and absorbance of the probe pulse were extracted from an interference pattern created by the probe and reference pulses and plotted as functions of the time delay *Δt* between the pump and probe pulses. This method enabled us to study ε variation due to the third-order non-linearity, free charge carriers excitation and their subsequent trapping at the energy levels in the bandgap.
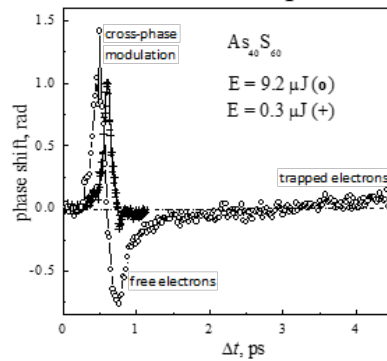
Fig.1 Phase shift of the probe pulse due to the cross-phase modulation by the pump pulse, free electrons excitation due to the two-photon absorption of the pump pulse, the electrons recombination and trapping.

Temporal dynamics of the non-linear optical response depends on the pump pulse energy E (Fig.1). At low E, density of free electrons in the conduction band is small, and ε varies mainly due to the third-order nonlinearity. Thus, values of the non-linear optical coefficients of refraction n_2 and absorption $β_2$ can be found by solution of the system of equations:

$$\partial I_{pu} / \partial z = -(\alpha + \beta_2 I_{pu})I_{pu}$$
$$\partial I_{pr} / \partial z = -(\alpha + 2\beta_2 I_{pu})I_{pr}$$
$$\partial \varphi_{pr} / \partial z = 2k\, n_2 I_{pu} \tag{1}$$

where I*pu* is the pump pulse intensity, I*pr* and φ*pr* are the probe pulse intensity and phase at the laser beam axis, *k* is the wavenumber, *α* is the single-photon absorption coefficient.

Glass compositions $As_{40}Se_{60-x}S_x$ with x = 0, 10, 15, 20, 30 were irradiated by the 50 fs pump pulse with the peak wavelength λ_p= 790 nm at their Urbach tails (ratio of the laser photon energy to the bandgap energy R = 0.78 − 0.9). Compositions with x = 40, 45,60 were irradiated outside their Urbach tails (R = 0.66 − 0.74). For all these compositions, the obtained n_2 magnitudes were positive and of the order of ~ 10^{-15} cm²/W unlike the direct-gap crystalline semiconductors having $n^2 < 0$ near their bandgap frequencies [3].

(2)

$$\Delta n(r,t) \approx \frac{e^2}{2n_0\varepsilon_0}\left\{-\frac{n_e(r,t)f_B}{m*\omega^2} + \frac{n_r(r,t)f_r}{m(\omega_r^2 - \omega^2)}\right\}$$

At higher E, refractive index n(r,t) varies also due to the charge carriers dynamics [2]: Here n_e and n_{tr} are electron density in the conduction band and at a trap level in the bandgap, f_{cb} and f_{tr} are oscillator strengths for the conduction band and for the trap level, ω is laser frequency, ω_{tr} is frequency of the transition associated with the trap level, m and e are mass and charge of electron, $m*$ is effective mass of electron in the conduction band, ε_0 is the vacuum permittivity, n_0 is linear refractive index. If λ_p is located near the FAB edge of a glass sample at the Urbach tail, time t_e of the photoexcited electrons transitions from the free state to a trap level does not depend on E, but te decreases with increasing R. In $As_{40}Se_{60-x}S_{15}$ sample, the trapping is so fast that excitation of free electrons has not been observed. If λ_p is located far from the FAB edge of a glass sample outside the Urbach tail, te decreases with increasing E. In this case, carriers dynamics develops as a two-steps process [2]: a hole trapping followed by an electron trapping by the self-trapped hole (Fig.2.)
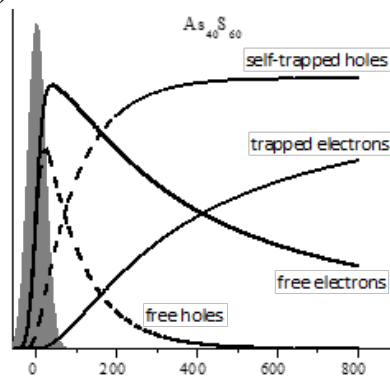
Fig.2 Schematic of the 50 fs laser pulse induced evolution of the charge carrier densities. The laser pulse is shown by the grey shadow.

In summary, peculiarities of the non-linear optical response of chalcogenide glasses of the system As-S-Se have been identified by analysis of ε evolution measured with the femtosecond resolution in time.

[1] A. Zakery, S.R. Elliot, Optical nonlinearities in chalcogenide glasses and their applications (Springer-Verlag, Berlin, Heidelberg, New York, 2007)
[2] S.S. Mao, F. Quere, S. Guizard, X. Mao, R.E. Russo, G. Petite, P. Martin Appl.Phys.A 79 1695 (2004)
[3] E.A. Romanova, A.I. Konyukhov, V. Kochubey, T.M. Benson, E. Barney, N. Abdel-Moneim, D. Furniss A.B. Seddon, S. Guizard, in Proc. of: Int. Conf. on Optical, Optoelectronic and Photonic Materials and Applications (ICOOPMA), at Journal of Physics: Conference Series, 619 (2014)

CALIBRATION OF MINIATURE PRISM-BASED STEREOSCOPIC IMAGERS FOR PRECISE SPATIAL MEASUREMENTS

Alexander S. Machikhin[1], Alexey V. Gorevoy[1,2]

[1]Scientific and Technological Center of Unique Instrumentation of Russian Academy of Sciences, 15, Butlerova str., Moscow, Russia

[2]Bauman Moscow State Technical University, 5/1, 2-ya Baumanskaya str., Moscow, Russia

gorevoy.a@gmail.com

Industrial videoendoscopes are widely used for remote visual inspection of aviation and rocket engines, nuclear equipment and many other industrial objects. Endoscopic measurement technologies based on stereoscopic and other methods allow simultaneous visual inspection and 3-dimensional (3D) spatial measurements of the detected defects.

The stereoscopic technique requires at least two images registered from different viewpoints with two imagers or one moving imager [1-3]. Modern industrial endoscopes may be equipped with the attachable stereo adapters which make it possible to obtain images from two different viewpoints on the single CCD sensor [4,5]. Such an adapter contains a biprism and auxiliary lens as shown in fig. 1 [6].
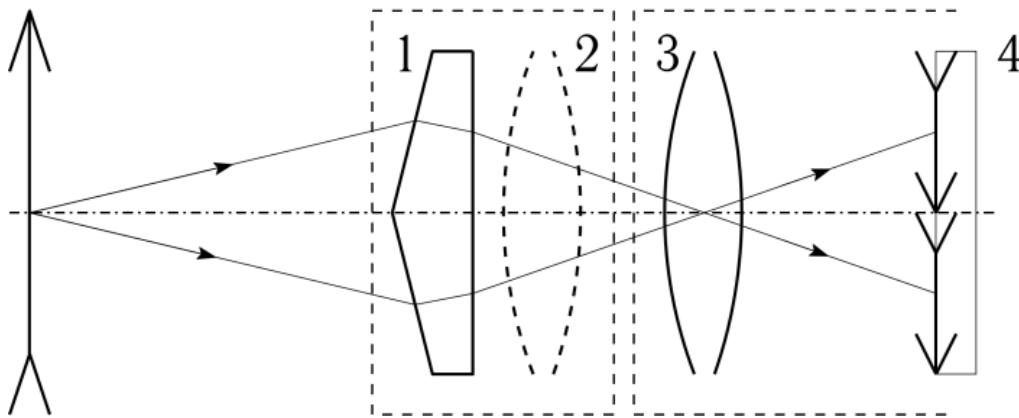
Fig. 1. Endoscope with stereo adapter: 1 —biprism, 2 — auxiliary lens, 3 —main lens, 4 — CCD sensor, 5 — attachable adapter, 6 — endoscope camera head coordinates

The conventional calibration methods [7,8] assume projective camera and polynomial distortion model, these algorithms are well described. The prism-based stereoscopic imager can be considered as two virtual cameras, their intrinsic and extrinsic parameters can be derived from the prism and main lens parameters as shown in [9-11]. This approach is unsuitable for precise measurements because the optical prism distortion is ignored. Additionally, the conventional camera model and the calibration procedure should be adapted for endoscope with attachable stereo adapter to consider the uncertainty of the attaching mechanism and the fact that simultaneous calibration of the adapter and the camera head is not always available [12].

This work is targeted to find the optimal mathematical model and the calibration algorithm for the prism-based stereoscopic imager. We proposed three types of camera models with polynomial distortion approximation and compared them with the ray tracing model based on the vector form of Snell law similar to the model used in [13]. Using the same approach as [14,15], the projection from 3D object coordinates to 2D image coordinates is regarded as the combination of simple transformations (Euclidean, affine, projective and polynomial). Our analysis identified

the main problems for these models, such as entrance pupil shift, non-homocentric beams and required number of coefficients for polynomial models and the iterative forward ray aiming for the ray tracing model. In order to evaluate each of the proposed models we have developed the software for the imitation of various calibration procedures using different types of calibration targets (such as boards and corners [2,7] or steps [16]). The input data (2D image) for calibration procedures is generated with full ray tracing model and high-order polynomial distortion model and additive noise. Then the estimated parameters for every model are used to calculate the uncertainty of 3D coordinates for the set of points distributed in the working volume, the average deviation and the maximum absolute deviation are the main criteria for model optimality. Furthermore,we applied this technique to find the number of coefficients for polynomial models required to reach desired measurement accuracy. The proposed method is flexible and suitable for different calibration algorithms and calibration targets. It can also be used to test stability and convergence for parameter optimization during the calibration procedures and to compare different calibration targets and strategies. inally, we conducted the experiments with a real industrial videoendoscope and attachable stereo adapter to validate the proposed method and confirmed its accuracy and effectiveness by comparison of the experimental results and computer simulation.

[1] R.I. Hartley and A. Zisserman, Multiple View Geometry, (Cambridge University Press, Cambridge, 2000)

[2] D.A. Forsyth and J. Ponce, Computer Vision: a Modern Approach, (Prentice-Hall, Upper Saddle River, 2012)

[3] A.V. Gorevoy, A.S. Machikhin, and A.M. Perfilov, Sci. and Tech. J. of Inf.Technology, Mechanics and Optics 4(92), 140–8 (2014)

[4] http://www.ge-mcs.com/download/RVI/XLG3/GEIT-65043EN_xlg3ds-lo.pdf

[5] http://www.olympus-ims.com/en/.downloads/download/?file=285212976

[6] A.S. Machikhin and V.I. Batshev, Eng. J.: Science and Innovation 7(19), http://engjournal.ru/catalog/pribor/optica/832.html

[7] Z. Zhang, IEEE Trans. on Pat. Anal. and Mach. Intel. 22(11), 1330–34 (2000)

[8] http://docs.opencv.org/modules/calib3d/doc/camera_calibration_and_3d_reconstruction.html

[9] D.H. Lee and I.S. Kweon, IEEE Trans. on Rob. and Autom. 16(5), 528-41 (2000)

[10] X. Yong, Single-lens multi-ocular stereovision using prism, (National University of Singapore, 2006)

[11] W.L. Kee, K.B. Lim, and D.L. Wang, J. of Elec. Sci. and Tech. 10(2), 97-101 (2012)

[12] S. Nakano, F. Hori, and K. Ogawa, US Patent US20100004507A1 (2010)

[13] Y. Takata, T. Torigoe, E. Kobayashi, and I. Sakuma, 7th Asian-Pacific Conf. on Med. and Biol. Eng. IFMBE Proc. 19, 750-3 (2008)

[14] J. Kannala and S.S. Brandt, IEEE Trans. on Pat. Anal. and Mach. Intel. 28(8), 1335-40 (2006)

[15] C. Wu, B. Jaramaz, and S.G. Narasimhan, Int. J. of Comp. Aided Surgery 15, 19-31(2010)

[16] http://www.ge-mcs.com/download/RVI/XLG3/XA-STCAL-MAN_RevC.pdf

ACOUSTO-OPTICAL METHOD   FOR FULL-FIELD HIGH TEMPERATURE MEASUREMENT

Alexander S. Machikhin, Pavel V. Zinin

Scientific and Technological Center of Unique Instrumentation of Russian Academy of

Sciences, 15, Butlerova str., Moscow, Russia

aalexanderr@mail.ru

The laser heating is one of the main tools in studying of mineral and synthesis of new materials under high pressure and high temperature in a diamond anvil cell [1,2]. One the main problem of the laser heating technique is that laser generates strong gradients of temperature in a specimen [3]. Further progress in the development of the laser heating techniques requires the knowledge of the temperature field in a material induced by the laser beam irradiation.

Under laser heating temperatures up to several thousand degrees can be achieved [1]. Usually the temperature is calculated from the radiation emitted from a material heated by the laser using Planck's blackbody equation [4,5]. If a regular spectrometer is used to measure radiation emitted from a heated material then such measurements only provide the temperature of the heated spot averaged over its area. That is why this method works perfectly only for a uniform temperature distribution. However, the temperature under laser does not have a uniform distribution. Two-dimensional temperature mapping of laser heated diamond anvil cell samples is performed by processing a set of four simultaneous images of the sample, each obtained at a narrow spectral range [6]. The disadvantage of this system is that it requires serious efforts to align the system in order to achieve perfect matching of the images obtained at different wavelengths. Because of that such a system has been installed in only a few laboratories.

In this study, we report on the development of a novel multispectral imaging radiometry system to measure 2-dimensional temperature distribution over the surface of an inspected object. It is experimentally demonstrated that the use of an imaging acousto-optic tunable filter synchronized with a CCD camera allows measurement of the temperature distribution over the surface of an inspected object and can be applied for thermal control of a specimen in a LH-DAC setup.

[1] V. B. Prakapenka, A. Kubo, A. Kuznetsov, A. Laskin, O. Shkurikhin, P. Dera, M. L. Rivers and S. R. Sutton, High Pres. Res. 28, 225-235 (2008).
[2] W. A. Bassett, Rev. Sci. Ins. 72, 1270-1272 (2001).
[3] A. Kavner, and W. R. Panero, Physics of the Earth and Planetary Interiors 143-44, 527-539 (2004).
[4] A. P. Jephcoat, and S. P. Besedin, Philosophical Transactions of the Royal Society of London Series a-Mathematical Physical and Engineering Sciences 354, 1333-1360 (1996).
[5] A. N. Magunov, Instruments and Experimental Techniques 52, 451-472 (2009).
[6] A. J. Campbell, Rev. Sci. Ins. 79, 015108 (2008).

RAMAN SCATTERING AND FLUORESCENCE OF GRAPHITIC PHASES FROM B-C-N TRIANGLE

Pavel V. Zinin

Scientific and Technological Center of Unique Instrumentation,

Russian Academy of Sciences, 15, Butlerova, Moscow, Russia

zosimpvz@yahoo.com

Graphene as the two-dimensional monolayer form of sp2-hybridized carbon, has attracted widerange interest due to its promising applications in electronic devices and composite materials. Naturally the assumption that graphenes from the B-C-N atomic composition triangle (Fig 1) possess many interesting properties is valid. Bulk single B-C-N hetero-graphene phases have not yet been obtained, however, we can study some of their properties using graphitic B-C-N phases. In this presentation, theory and experimental measurements of the Raman scattering of the graphitic phases from the B-C-N triangle is discussed.
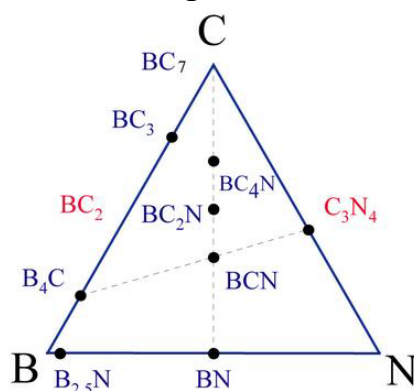
Fig. 1. The composition triangle in the BC-N system.
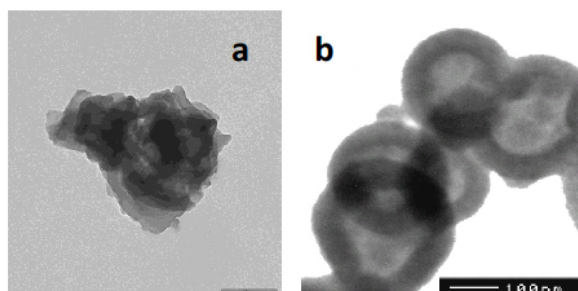
Fig.2. TEM images of the graphitic (a) and spherical (b) modifications of carbon nitride C3N4.

Carbon: A typical Raman spectrum of the graphite consists of two main peaks referred to as D (1357 cm^{-1}) and G (1560) peaks and can be detected by visible Raman scattering.

C-N phases: The Raman spectrum of the graphitic C_3N_4 phase (g-C_3N_4) can be measured only by ultraviolet Raman scattering because of strong fluorescence. The UV Raman spectrum of the g-C_3N_4 is substantially different from that of graphite. It has two strong peaks at 691 cm^{-1} and 988 cm^{-1} assigned to different types of ring (s-triazine ring) breathing modes. Measurements of the fluorescence spectra and quantum yield (QY) of graphitic (g-C_3N_4) and spherical (s-C_3N_4) modifications (Fig. 2) of carbon nitride showed a strong dependence of the nanostructure on the fluorescence intensity of the carbon nitride modifications and revealed unusually high values of the fluorescence QY for s-C_3N_4, up to 32% with a 532 nm excitation laser. It was found that the

intensity of the fluorescence at the maximum is two orders as high for s-C_3N_4 as for g-C_3N_4.

B-C phases: A typical Raman spectrum of the BCx phase material has two broad peaks at 1364 cm^{-1} and 1573 cm^{-1}, which are characteristic for amorphous carbon and denoted usually as D- and G- bands, respectively. Theoretical simulation shows that the G band energy remains somewhat constant as a function of the boron concentration (x). On the contrary the D band energy shows a distinctive change depending on the boron concentration--decreasing with increasing B concentration.

MECHANISMS OF TISSUE OPTICAL IMMERSION CLEARING

Elina A. Genina, Alexey N. Bashkatov, Valery V. Tuchin

Research-Educational Institute of Optics and Biophotonics, Saratov State University, 83 Astrakhanskaya str., Saratov 410012, Russia

Interdisciplinary Laboratory of Biophotonics, Tomsk State University, 36 Lenin Avenue,

Tomsk 634050, Russia

eagenina@yandex.ru

During the last 25 years the interest to the development and application of optical methods in clinical functional imaging of physiological conditions, diagnostics and therapy of cancer, and other diseases grows due to the unique informativity, relative simplicity, safety, and sufficiently low cost of optical instruments [1]. However, the main limitation of optical diagnostic methods, including the optical diffusion tomography, optical coherence tomography, confocal microscopy, reflection spectroscopy, etc., is the strong scattering of light in biological tissues and blood that reduces the contrast, spatial resolution, and probing depth [2]. One of simple and efficient methods of solving the problem, is the temporary reduction of the tissue light scattering [1-3].

We discuss the physical and molecular mechanisms of immersion method of optical clearing of fibrous tissues. The optical immersion clearing is based on the impregnation (immersion) of the tissue with a biocompatible chemical agent (optical clearing agent -OCA), possessing sufficiently high refractive index to match the refractive indices of the scatterers and the surrounding medium, penetrating into the interstitial liquid of the tissue.
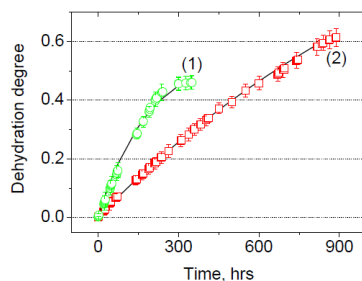
Fig. 1. Dehydration kinetics of human skin samples under the action of 88% glycerol solution (1) and in the course of interstitial water evaporation in air (2) [1]

At present, several physical and chemical mechanisms of the light scattering reduction under the action of OCA are proposed and thoroughly described [1-9]: dehydration of tissue components, partial replacement of interstitial fluid with the immersion agent, and structure modification or dissociation of collagen. The first mechanism is related to the hyperosmotic properties of the OCA. The contact of hyperosmotic OCA with the tissue surface causes the water diffusion from the tissue (Fig.1). These processes produce fast and considerable clearing effect, since, first, the concentration of salts and proteins dissolved in the interstitial fluid increases and, therefore, the refractive index of the interstitial fluid becomes closer to that of the scattering fibrils, and, second, the weight and the thickness of the tissue decrease, the tissue becomes denser, and the ordering of scattering components increases [3, 6].

For fibrous tissues, such as sclera, dura mater, dermis, etc., both processes, namely, the water loss and the diffusion of the hyperosmotic agent into the skin, occur simultaneously, but the

mechanism of the interstitial fluid replacement with the OCA solution is prevailing for all the agents used, since their molecular size is much smaller than the mean separation between the fibrils [1, 3, 5]. The collagen fibres have complex selforganising structure. It is established that the hydrogen bond is the main bonding force between the triple collagen helices. The OCAs with multiple hydroxyl groups possess a greater negative charge that destabilises the highly-ordered collagen structure till its dissociation (Fig. 2). Since the hydrogen bonds in the triple
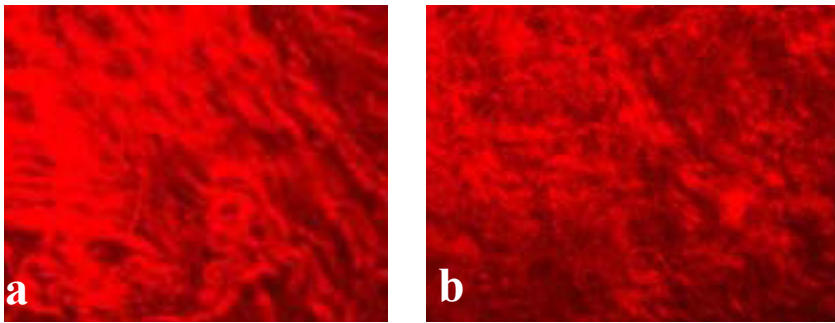
Fig. 2. The packing density change of collagen fibres in the rat skin ex vivo under the action of 50% aqueous solution of polyethylene glycol: the initial state (a) and in 15 minutes after the application of OCA (b). The images were obtained by means of second harmonic generation microscopy [1]

collagen helices belong to non-covalent interactions, the OCA-induced effect on the collagen dissociation can be easily reversed [8, 9].

Mathematical modelling of molecular dynamics in order to clarify the formation of hydrogen bonds between the alcohol (glycerol, xylitol, and sorbitol) and collagen molecules was shown that the bridges with large number of carbon atoms in the hydrogen bond bridge, built in between the collagen molecules in the helix, can break the collagen-collagen and collagen-hydroxyl bonds more efficiently than the bridges with smaller numbers [7].

Thus, administration of OCAs allows scientists to effectively control the optical properties of tissues. The control allows for increasing efficacy for the application of ifferent optical imaging and spectroscopic (optical biopsy) techniques for medical purposes. The immersion technique also has great potential for a number of therapeutic and surgical methods using laser-beam action on a target area hindered within the tissue [1-3].

[1] E. A. Genina, A. N. Bashkatov, Yu. P. Sinichkin, I. Yu. Yanina, and V. V. Tuchin, Journal of Biomedical Photonics & Engineering, 1(1), 22-58 (2015).
[2] V. V. Tuchin, Tissue Optics: Light Scattering Methods and Instruments for Medical Diagnosis (SPIE Press, Bellingham, 2015).
[3] D. Zhu, K. Larin, Q. Luo, and V. V. Tuchin, Laser & Photonics Reviews, 7(5), 732-757 (2013).
[4] C. Drew, T. E. Milner, and C. G. Rylander, J. Biomed. Opt., 14(6), 064019 (2009).
[5] Z. Mao, D. Zhu, Y. Hu, X. Wen, and Z. Han, J. Biomed. Opt., 13, 021104 (2008).
[6] D. K. Tuchina, R. Shi, A. N. Bashkatov, E. A. Genina, D. Zhu, Q. Luo, and V. V. Tuchin, J. Biophotonics, 8(4), 332-346 (2015).
[7] J. M. Hirshburg, K. M. Ravikumar, W. Hwang, and A. T. Yeh, J. Biomed. Opt., 15(5), 055002 (2010).
[8] A. T. Yeh, and J. Hirshburg, J. Biomed. Opt., 11(1), 014003 (2006).
[9] A. T. Yeh, B. Choi, J. S. Nelson, and B. J. Tromberg, J. Invest. Dermatol., 121,1332–1335 (2003).

IRIDIUM NANOPILLAR ARRAYS FOR HIGHLY REPRODUCIBLE SURFACE-ENHANCED RAMAN SPECTROSCOPY (SERS)

Antti Matikainen[1], Tarmo Nuutinen[2], Guoguo Kang[3], Seppo Honkanen[1], Pasi Vahimaa[1]

[1]*Institute of Photonics, University of Eastern Finland, Joensuu, Finland*

[2]*Department of Biology, University of Eastern Finland, Joensuu, Finland*

3*School of optoelectronics, Beijing Institute of Technology, Beijing, China*

antti.matikainen@uef.fi

Surface-enhanced Raman spectroscopy (SERS) sensors have been a matter of great interest in academic research for decades. Thus, a variety of different gold and silver nanostructures have been proposed over the years as "ideal" SERS substrates that can provide both high signal enhancement and consequently also high measurement sensitivity. Despite the extensive research however, the use of SERS as an analytical tool is still currently quite limited, mainly because it is notoriously difficult to perform repeatable SERS measurements. These difficulties originate from the fact that it is extremely demanding to fabricate SERS nanostructures from gold or silver with nanometer scale precision, which is essential, if truly reproducible measurements are desired.

Here we propose a fabrication approach that can provide high signal enhancement without compromising the repeatability of the measurements. The concept [1] is based on an array of nanopillars coated with iridium by using atomic layer deposition (ALD). Due to the high precision deposition and the resulting, extremely ordered distribution of hot spots, the enhancement generated by the structures is highly reproducible with only ±4% signal intensity variation. Furthermore, the signal enhancement is also significant and its magnitude actually rivals the
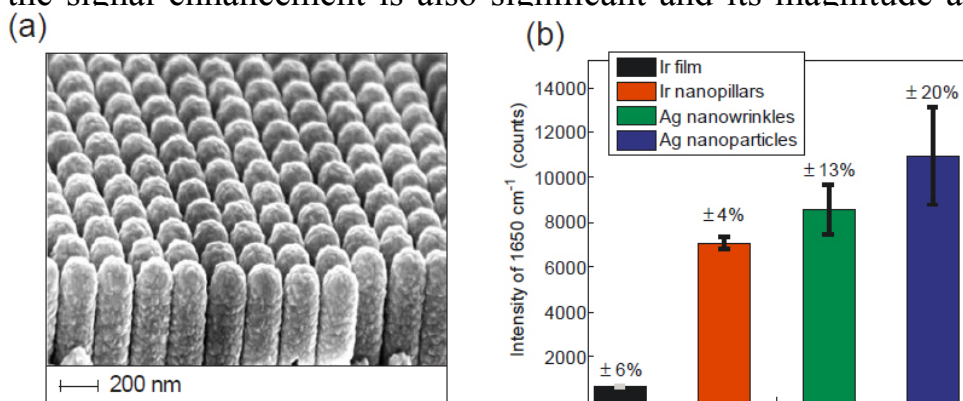
enhancement obtained with different silver substrates we have reported earlier [2,3].

Fig. 1. (a) SEM image of the ALD coated iridium nanopillar structures. (b) SERS performance comparison against different silver based substrates.

[1] G. Kang, A. Matikainen, P. Stenberg, E. Färm, P. Li, M. Ritala, P. Vahimaa, S.Honkanen, and X. Tan, ACS Appl. Mater. Interfaces, 7, 11452 (2015).
[2] A. Matikainen, T. Nuutinen, P. Vahimaa, S. Honkanen, Sci. Rep. 5, 8320 (2015).
[3] H. Stenberg, A. Matikainen, S. Daniel, T. Nuutinen, P. Stenberg, S. Honkanen, T. Pakkanen, P. Vahimaa, M. Suvanto, Macromol. Mater. Eng. 300, 386 (2015).

FROM SILVER CHLORIDE INTERMEDIATE TO SERS APPLICATIONS

Tarmo Nuutinen[1,2], Antti Matikainen[1], Seppo Honkanen[1], Pasi Vahimaa[1]

[1]Institute of Photonics

[2]Department of Biology, University of Eastern Finland

tarmo.nuutinen@uef.fi

Metallic silver is prone to oxidation in ambient atmosphere and this limits its use in the plasmonic and SERS applications. Also, depending on the application, metallic nanostructures can be difficult to fabricate – especially onto a tip of optical fibre. By using silver chloride as an intermediate, we can go around these obstacles.
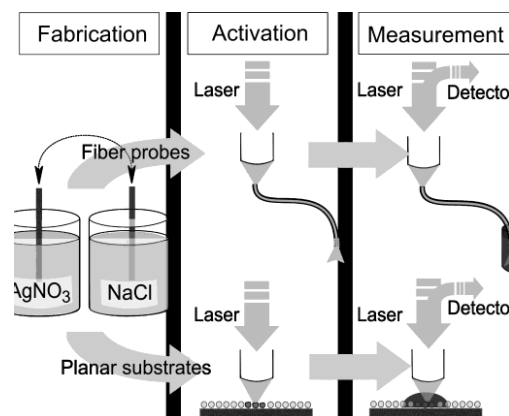
The fabrication is simply done by immersing the probes (or substrates) by turns to dilute solutions of AgNO3 and NaCl (Fig.1)[1]. The size of forming AgCl crystals is commensurate to the number of cycles of immersions (Fig.2, left halves of the images).
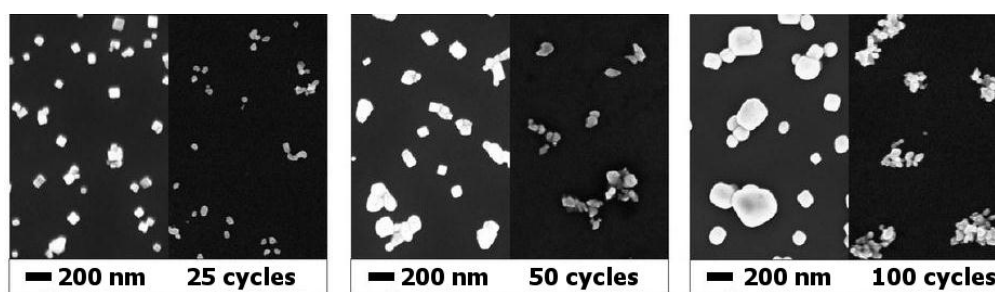
Fig. 2. AgCl crystals and Ag structures after the activation

Prior to measurements, AgCl needs to be activated i.e. turned to SERS active metallic silver. This is simply done by the light from a SERS instrument. In this photoreduction, crystals collapse into elaborate Ag structures (Fig.2, right halves of the images).

In the measurements, freshly activated probes are used and when immersed in a sample solution, as low as <5 nM analyte (e.g. Rh6g) concentrations can be easily detected.

The signal intensities are dependent on the number of cycles (Fig. 3A) i.e. on the original crystal sizes of the crystals (Fig. 2A).

When the probes are stored in the inactive stage, they are resistant to the atmospheric oxidation (Fig. 3B), providing a solution to the poor shelf-live and repeatability of regular SERS probes & substrates.
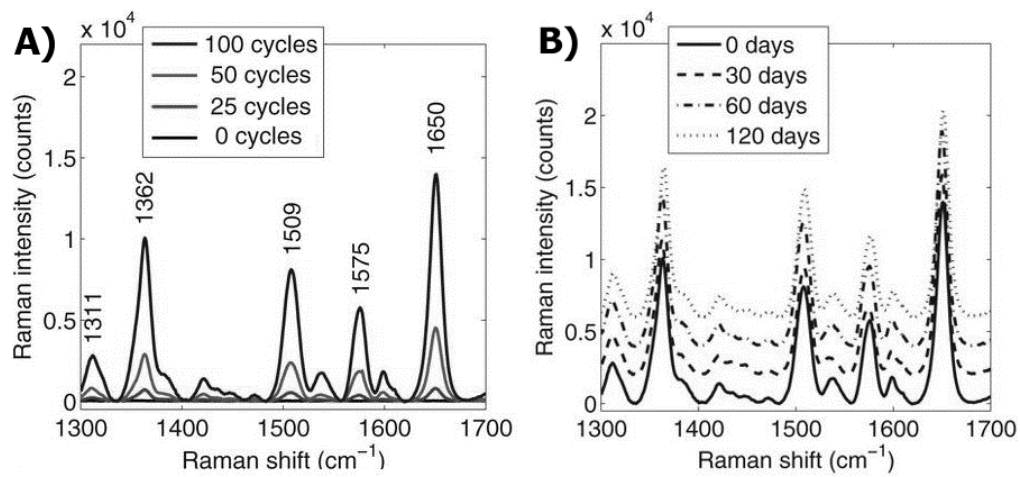
Fig. 3. A) Signal intensities by the cycle number and B) by the time being stored in inactivated, the intermediate stage. Note the spectra (B) have been displaced for clarity.

[1] Matikainen A, Nuutinen T, Vahimaa P and Honkanen S (2015). A solution to the fabrication and tarnishing problems of surface enhanced Raman spectroscopy (SERS) fiber probes. Scientific Reports, 5, Article number: 8320, doi:10.1038/srep08320

EFFECT OF TEMPERATURE AND VISCOSITY ON THE QUANTUM YIELD OF THE MULTI - ENZYME SYSTEM LACTATE DEHYDROGENASE + NAD(P)H:FMN-OXIDOREDUCTASE COUPLED WITH BACTERIAL LUCIFERASE

Maria S. Nemchinova[a], Oleg S. Sutormin[a], Irina E. Sukovataya[a], Valentina A. Kratasyuk[ab]

[a]Department of Biophysics, Institute of Fundamental Biology and Biotechnology, Siberian Federal University, 79 Svobodny pr., Krasnoyarsk, 660041, Russia; [b]Institute of Biophysics, Russian Academy

nemchinova.marya@yandex.ru

One of the main problem of the modern biophysics is studying cells how sustainable, self-regulating, holistic mechanism. In cells, multi - enzyme systems work cooperatively to direct the formation of desired products within the defined compartmentalization of a cell. Numerous researches are devoted to the modeling in vivo-like environment in a tube and its impacts on enzyme activity.

Modification of the intracellular microenvironment by variety of physical and chemical properties of reaction media and immobilization techniques is one of the latest strategies aimed at full structural and functional stabilization of biomolecules [1].

The protein–solvent interaction is a problem concerning the understanding of enzyme catalysis mechanisms too, since the solvent alters inter- and intra-molecular electrostatic and hydrophobic interactions. A perspective approach in the study of interaction types at the formation of enzyme–substrate complexes is the addition of organic solvents in a reaction medium [2]. Among all macromolecules a crowding agents as glycerol and sucrose are commonly used to investigate macromolecular processes, such as protein thermal stability, kinetics of protein unfolding and / or refolding, self-assembly, and aggregation [3]. Experimental models in the presence of glycerol and sucrose imitate enzymes activity in natural microenvironment, but have different chemical nature (disaccharide and polyol).

A unique object for this task is bioluminescent multi-enzyme systems based on bacterial luciferase in which the chemical bond energy is converted into light. The coupled multi-enzyme system lactate dehydrogenase + NAD(P)H:FMN-oxidoreductase + bacterial luciferase emits light at 445 nm in the presence of FMN, NAD(P)H, a long-chain aliphatic aldehyde and molecular oxygen. The main characteristics of the bioluminescent reaction are the following kinetic parameters of the light flash: maximum reaction rate (I0), quantum yield (Q) and light emission decay constant (kdec). Moreover, this is extremely important develop physico-chemical basis of bioluminescence assay, which extended the scopes of bioluminescence assay, increased luciferase activity and thermal stability [4].

The aim of this work was to examine the influence viscosity of reaction media on the thermal stability and kinetics of the multi-enzyme system lactate dehydrogenase + NAD(P)H:FMN-oxidoreductase coupled with bacterial luciferase.

Thermal stability of the multi-enzyme system in buffer and in the presence of glycerol and sucrose was determined by variation of the maximal luminescence intensity and light emission decay constant after incubation of the enzyme preparations at different temperatures (15-80°C) for min.

The impact of glycerol and sucrose on the catalytic activity of the multi-enzyme system was detected through the ratio of the maximum luminous intensity in their presence to the maximum luminous intensity of the control (I_i/I_0) and through changes in the time needed to reach the maximum luminescence (t_{max}) in their presence, as compared to the control. Each experimental point was measured in at least five measurements.

Addition of organic solvents into the reaction media of the coupled bioluminescent reaction change the kinetic parameters of the light flash: maximum reaction rate (I_0), quantum yield (Q) and light emission decay constant (k_{dec}).

The results showed that crowding agents as glycerol and sucrose in reaction media influence on kinetic dependence curve of the multi-enzyme bioluminescence system. In the presence of glycerol and sucrose in the reaction media kinetic dependence curve of the bioluminescence reaction begins with the substantial diminution of the intensity of the luminescence of multi-enzyme system, this result differs from the buffer there were measured the monotonic increase of the intensity of the luminescence of the system. The similar kinetic dependences curves were measured for all used concentrations of glycerol and sucrose. One can assume that the nature of crowding agents does not impact on the kinetic dependences curves of the multi-enzyme bioluminescence system.

The quantum yield - total number of photons released in the course of reaction calculated from intensity and the rate constant is affected by the variation of both these reaction parameters. The value of Q increases with addition of sucrose and decreases in the presence of glycerol. The value of the quantum yield of luminescence and a constant decay of coupled bioluminescent enzyme system do not depend on the viscosity of the reaction media.

The influence of the viscosity of the reaction medium on the thermal stability and thermal inactivation kinetics of the multi - enzyme system lactate dehydrogenase +NAD(P)H:FMN-oxidoreductase coupled with bacterial luciferase was investigated.

It was shown that in the presence of crowding agents the kinetics activity of the multi-enzyme system decreases. For example, with viscosity 0,5-1,3 cP approximately decreases the maximum luminous intensity (I_{max}) by 50 times. The optimum temperature of the multi- enzyme system in buffer and with viscosity 0,5-1,3 cP observed at 30°C. A further increasing the viscosity (1,76-6 cP) leads to decreasing the maximum luminous intensity (I_{max}) of the multi-enzyme system by 5-7 times and the brightly expressed optimum temperature of the multi-enzyme system is not observed, i.e. the system becomes more resistant to the effects of high temperatures. Sucrose stabilizes long-lived intermediate of bioluminescent reaction. This might be due to the fact that high concentrations of sucrose stabilize the native structure of a protein in aqueous solutions [5].

The results will be useful for development of a new class of high-sensitive enzymatic assays that could resist chemical and physical extremes and stay consistently active during storage.

[1] V. M. Balcão and M. M. Vila, Adv. Drug Deliv. Rev. 14, 213–220 (2014).
[2] O. S. Sutormin, I.E. Sukovataya, and V.A. Kratasyuk, Luminescence 29, (2014).
[3] M. Feig, Modeling Solvent Environments: Applications to Simulations of Biomolecules, 1st ed., (Wiley, New York, (2010).
[4] O. S. Sutormin, I.E. Sukovataya, and V.A. Kratasyuk, Luminescence 27, (2012).
[5] J. C. Lee and S. N. Timasheff, Biochemistry 256, 7193-7201 (1981).

UV LASER-INDUCED FLUORESCENCE SPECTROSCOPY AND LASER-DOPPLER FLOWMETRY IN THE DIAGNOSTICS OF ALOPECIA

Diana P. Skomorokha, Yulia N. Pigareva, Vladimir V. Salmin

Krasnoyarsk State Medical University named after Prof. V.F.Voino-Yasenetsky, Russia, Krasnoyarsk, Partizana Zheleznyaka str., 1

Silverselena@list.ru

Development of optical biopsy methods has a great interest for medical diagnostics. In clinical and experimental studies it is very important to analyze blood circulation quickly and accurately, thereby laser Doppler flowmetry (LDF) is widely used. UV laser-induced fluorescence spectroscopy (UV LIFS) is express highly sensitive and widely-spread method with no destructive impact, high excitation selectivity and the possibility to use in highly scattering media.

The goal of this work was to assess a correlation of UV laser-induced fluorescence spectroscopy and laser Doppler flowmetry parameters, and a possibility to identify or to differentiate various types of pathological changes in tissues according to their autofluorescence spectra.

Three groups of patients with diffuse (symptomatic) alopecia, androgenic alopecia, and focal alopecia have been tested. Each groups consisted of not less than 20 persons. The measurements have been done in the parietal and occipital regions of the sculls. We used the original automated spectrofluorimeter to record autofluorescence spectra, and standard laser Doppler flowmeter BLF-21 (Transonic Systems, Inc., USA) to analyze the basal levels of blood circulation.

Our results show that UV LIFS accurately distinguishes the zones with different types of alopecia. We found high correlation of the basal levels of blood circulation and the integrated intensity of autofluorescence in the affected tissue.

SURFACE-ENHANCED RAMAN SPECTROSCOPY FOR ENZYMATIC ACTIVITY DETECTION

Nechaeva N.L., Kurochkin I.N.

Chemical Enzymology Department, Faculty of Chemistry, Lomonosov Moscow State University

Nechaeva.n.l@yandex.ru

Human cholinesterases (acetylcholinesterase AChE and butyrylcholinesterase BChE) have important physiological functions such as involvement in neural signal transmission [1] and stoichiometric capture of organophosphates [2,3]. There are many chemicals and drugs that affect the cholinergic nervous system: nerve agents, prophylactic antidotes, myorelaxants and other therapeutic drugs. Since thiocholine (TCh) is a hydrolysis product of human cholinesterases, its accumulation can represent enzymatic status in organism. Both abnormal low and high values of cholinesterase activity may be caused by some diseases, intoxication [4,5], and drug use [6]. Therefore the determination of thiocholine in blood with high accuracy is of great importance for clinical diagnostics.
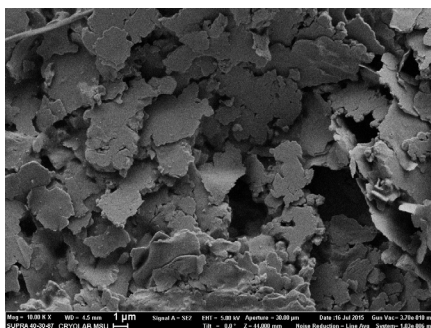
Figure 1. A typical SEM-image of silver substrate

At the present time, the electrochemical methods [7,8] are commonly used for the hiocholine detection due to low limit of detection (LOD) [9]. However, these methods have a number of limitations, such as the difficulty of a routine measure or need to record the baseline. Therefore the further development of detection techniques is actively studied. In this regard, surfaceenhanced Raman spectroscopy (SERS) is very promising in view of its ability to detect single molecules and simplicity of experiment and sample preparation.

One of the SERS-effect explanation is local increasing of electromagnetic field on the roughened surface of metal nanoparticles. New silver SERS-substrate was discovered, characterized and explored. It has roughened lamellar structure (Fig. 1) that is causing high intensity of Raman signal from analyte. New technique of TCh detection as well as technique of BChE activity detection was developed.
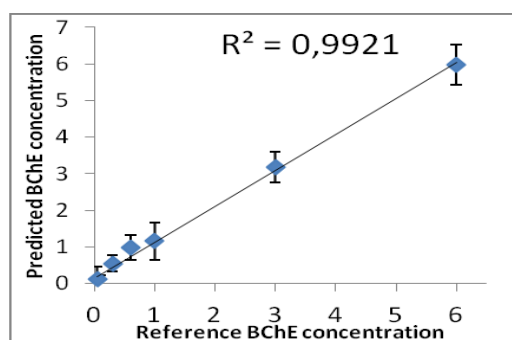
Figure 2. Calibration curve for BChE activity detection

Spectra of substrates (ATCh and BTCh) and product of enzymatic hydrolysis (TCh) were obtained, calibration curves of BChE were constructed (Fig. 2). This technique allows determination of BChE concentration and its activity in buffer and blood.

[1] T. Marrs Toxicology of organophosphate nerve agents, chemical warfare agents (Wiley, New York, 2007)

[2] J. Bajgar, British J. of Industrial Medicine 49, 648-653 (1992)

[3] B. Wilson and J. Henderson Reviews of Environ. Contamination and Toxicology 128, 55-69 (1992)

[4] H. Zejli, J. Hidalgo-Hidalgo de Cisneros, I. Naranjo-Rodriguez, B. Liu, K. Temsamani and J. Marty Talanta 77(1), 217-221 (2008)

[5] L. Zhang, A. Zhang, D. Du and Y. Lin Nanoscale 4(15), 4674-4679 (2012)

[6] R. Clark Insecticides: organic phosphorus compounds and carbamates (McGraw-Hill Professional 7th edn, New York, 2002)

[7] A. Eremenko, E. Dontsova, A. Nazarov and I. Kurochkin Thick film thiol sensors for cholinesterases assay (Military Publishing House, Sofia, 2014)

[8] A. Eremenko, E. Dontsova, A. Nazarov, E. Evtushenko, S. Amitonov, S. Savilov, L. Martynova, V. Lunin and I. Kurochkin Electroanalysis 24 (3), 573-580 (2012)

[9] I. Kurochkin, L. Sigolaeva, A. Eremenko, E. Dontsova, M. Gromova, E. Rudakova and G. Makhaeva Layer-by-layer electrochemical biosensors for blood esterases assay (Military Publishing House, Sofia, 2014.

PLASMON-RESONANT NANOPARTICLES WITH VARIABLE MORPHOLOGY FOR OPTICAL IMAGING

O. Bibikova[1], S. Prateek[1], I. Skovorodkin[1], A. Popov[1], A. Bykov[1], E. Panfilova[2], M. Kinnunen[1], V. Bogatyrev[2], S. Vainio[1], K. Kordas[1], N. Khlebtsov[2,3], V. Tuchin[1,3]

[1]University of Oulu, P.O. Box 4500, 90014, Oulu, Finland

[2]Institute of Biochemistry and Physiology of Plants and Microorganisms, Russian Academy of Sciences, Prospect Entuziastov, 13, 410049, Saratov, Russian Federation

[3]Saratov State University, Astrakhanskaya St., 83, 410012, Saratov, Russian Federation

Advances in development of plasmon-resonant nanoparticles (PRNPs) provide wide possibilities for researchers to apply PRNPs with variable forms in practically all biophotonic and biomedical applications, which is based on the unique physical and chemical properties of PRNPs, specifically by their plasmon resonance (PR) [1]. PR results in highly localized field enhancement at the PR wavelength as well as intense absorption and scattering of incident light. The ratio between the absorption and scattering properties is of high importance for PRNPs integration into biophotonics applications [2].

Here, we present the investigation of optical properties (scattering and absorption abilities) of PRNPs (naked or encapsulated in silica shells) with different morphologies. We compared the backscattering of nanospheres, nanostars, and nanocubes in living cells by the laser confocal microscopy in combined scattering and transmition light modes to eliminate the back-scattering signal of gold nanoparticles.

Scattering properties of PRNPs were investigated using optical coherence tomography (OCT) by imaging of nanoparticle suspensions in glass capillary to significantly increase capillariy visibility. The plasmon resonance of nanostructures corresponded to the central emission wavelength of the light source of the employed OCT.

We investigated the opportunity of cells transfection by the use of optoporation – generation a transient pore on the cell membrane. The cells were irradiated by a continuous wave laser (wavelength 808 nm) and a fibre-optic nanosecond 3-D scanning laser (wavelength 1064 nm, pulse duration 5 ns) in presence of nanospheres on nanostars in comparable size for enhanced cell membrane permeabilization and more efficient penetration of nanostructures into cells.

[1] L A. Dykman, N. G. Khlebtsov "Gold nanoparticles in biomedical applications: recent advances and perspectives", Chem. Soc. Rev., 41, 2256–2282 (2012).
[2] E. Chul Cho, C. Kim, F. Zhou, C. M. Cobley, K. H. Song, J. Chen, Z.-Yu. Li, L. V. Wang, Y. Xia, "Measuring the Optical Absorption Cross Sections of Au-Ag Nanocages and Au Nanorods by Photoacoustic Imaging," J. Phys. Chem. 113, 9023–9028 (2009).

THE MORPHOLOGICAL CHANGES IN TRANSPLANTED TUMORS OF RATS AT PLASMONIC PHOTOTHERMAL THERAPY

A.B. Bucharskaya,[1] G.N. Maslyakova,[1] N.A. Navolokin,[1] N.I. Dikht1, G.S. Terentyuk,[1,2] A.N. Bashkatov,[2,3] E.A. Genina,[2,3] B.N. Khlebtsov,[4] N.G.Khlebtsov,[4] V.V.Tuchin[2,3,5]

[1]Saratov State Medical University, Russia

[2]Research-Educational Institute of Optics&Biophotonics, Saratov State University, Russia

[3]Interdisciplinary Laboratory on Biophotonics, Tomsk State University, Russia

[4]Institute of Biochemistry and Physiology of Plants and Microorganisms RAS, Russia

[5]Institute of Precision Mechanics and Control, RAS, Russia

allaalla_72@mail.ru

Laser thermal therapy is commonly used in cancer treatment. The major limitation of such method of therapy is associated with low spatial selectivity. This restriction may be excluded by with using plasmon-resonant gold nanoparticles as photothermal sensitizers. The unique optical properties and low toxicity of gold nanoparticles make them promising therapeutic agents for cancer treatment. The considerable amount of studies was focused on the application of various gold nanoparticles for plasmonic photothermal therapy (PPTP). However, the choice of the most efficient and gentle methods of PPTT was an actual problem of experimental studies.

The aim of work was to study the morphological changes in transplanted liver tumors of rats after plasmonic photothermal therapy. Thirty male outbred albino rats with transplanted liver cancer PC-1 were used in the experiment. The experimental model of rat liver cancer was reproduced by transplantation of tumor cells suspension of liver cancer (cholangiocarcinoma line PC-1), obtained from the bank of tumor strains of Russian Cancer Research Center n.a. N.N. Blokhin. Suspension was implanted subcutaneously in rats. The experiments were conducted accordingly the guidance «International Guiding principles for Biomedical Research Involving Animals» [1]. When the tumor reached a diameter of 1.0 ± 0.2 cm3 the animals were randomly divided into three groups (10 rats in group): group 1 - without exposure, group 2 - with single gold nanorods injection and PPTT, group 3 - with double injection of gold nanorods and PPTT. The gold nanorods synthesized in the Laboratory of Nanobiotechnology (Institute of Biochemistry and Physiology of Plants and Microorganisms of Russian Academy of Sciences, Saratov, Russia) by previously established method [2] were used. To prevent nanoparticles aggregation in biological tissue and enhance biocompatibility nanoparticles were functionalized with thiolated polyethylene glycol (MW=5000, Nektar, USA) by previously established method [3]. Geometrical parameters of gold nanorods were determined from analysis of transmission electron microscopy (TEM) images (Libra-120, Carl Zeiss, Germany). Size of the nanorods was 41 ± 8 nm (length) and 10 ± 2 nm (diameter), and concentration of the nanorods in the suspension was 400 µg/ml, which correspond to optical density of 20 at 808 nm. The gold nanorods in a volume of 1 ml were injected intravenously singly and doubly once a day. After one day after injection the tumors were irradiated by the infrared 808-nm diode laser LS-2-N-808-10000 (Laser Systems, Ltd., St.-Petersburg, Russia) during 15 min at power density 2.3 W/cm2. Temperature control of the tumor heating was provided by IR imager IRI4010 (IRYSYS, UK). Prior medical procedure or treatment, the rats were anaesthetized with Zoletil 50 (Virbac, France) in dose of

0.05 mg/kg. The withdrawal of the animals from the experiment and sampling of tumor tissue for morphological study were performed 24 hours after the laser exposure. The standard histological and immunohistochemical staining with antibodies to proliferation marker Ki-67 and apoptosis marker BAX were used for morphological study of transplanted tumors. The determining of gold concentration was conducted in the 1 g of tumor tissue by atomic absorption spectroscopy on spectrophotometer Dual Atomizer Zeeman AA iCE 3500 (ThermoScientificInc., USA).

In the first group of rats the tumors had a lobed structure; segments were separated by thin layers of connective tissue. Tumor cells had oval-rounded shape with eccentrically located nuclei. A significant portion of cytoplasm was occupied by large vacuoles containing mucus. There were clusters of mucous masses in the intercellular spaces.

In second group of the rats (single nanoparticle injection and laser hyperthermia) the tumor temperature increased from 35°C up to 42°C. At atomic absorption spectroscopy the gold accumulation in the tumor tissue was insignificant (0.142 µg/g) and the temperature increasing was due to only laser hyperthermic influence. The tumor in the group kept lobed structure. There were small foci of necrosis (10-20% of the total area of tissue), the tumor cells with necrotic changes were noted. The single mitosis was identified. The vessels were full-blooded, there was thickening of the connective tissue septa and infiltration of leukocytes.

In third group of the rats (double nanoparticle injection and laser hyperthermia) we observed the increasing of tumor temperature (up to 46°C) at PPTT. The gold content in the tumor tissue increased almost 9 times (up to 1,236 µg/g) compared to group with single injection. The more pronounced necrotic changes were revealed in the tumor tissue after PPTT. The tumor cells with degenerative changes persisted only in subcapsular zone, tumor necrosis occupied up to 60-70% of area of the slice. The decreasing of the proliferation marker Ki-67 expression and increasing of the apoptosis marker BAX expression were observed after double intravenous injection of gold nanorods and PPTT.

The experiments showed that the double injection of gold nanorods and laser hyperthermia on tumor-bearing liver in laboratory animals has more pronounced damaging effect expressed in necrotic and degenerative changes in the tumor cells. The decreasing the proliferation marker Ki-67 and the increasing expression of the apoptosis marker BAX were observed after PPTT.

[1] International Guiding Principles for Biomedical Research Involving Animals http://www.cioms.ch/index.php/12-newsflash/227-cioms-and-iclas-release-the-new-international-guiding-principles-for-biomedical-research-involving-animals, (CIOMS&ICLAS, 2012).
[2] A.V. Alekseeva, V.A. Bogatyrev, B.N. Khlebtsov, A.G. Melnikov, L.A. Dykman, N.G. Khlebtsov, Colloid Journal. 68, 661 (2006).
[3] B. N. Khlebtsov, E. S. Tuchina, V. A. Khanadeev, E. V. Panfilova, P.O. Petrov, V.V. Tuchin, N. G. Khlebtsov, J. Biophotonics. 6, 338 (2013).

MONITORING PROPERTIES OF BIOLOGICAL TISSUES USING [Y$_2$O$_3$:Yb, Er] UPCONVERSION PARTICLES

Elena Volkova[1,2], Irina Yanina[1,2,3], Alexey Popov[2], Alexander Bykov[2], Alexander Skaptsov[1], Marina Kozintseva[1], Julia Konyukhova[1], Vyacheslav Kochubey[1], Igor Meglinski[2], Valery Tuchin[1,2,4]

[1]*Saratov State University, Research-Educational Institute of Optics and Biophotonics, Saratov, Russia*

[2]*University of Oulu, Optoelectronics and Measurement Techniques Laboratory, Oulu, Finland*

[3]*Saratov State Medical University, Department of Medical and Biological Physics Saratov, Russia*

[4]*Laboratory of Laser Diagnostics of Technical and Living Systems of Precise Mechanics and Control Institute of the Russian Academy of Sciences, Saratov, Russia*

volkovae87@gmail.com

The results of real-time local temperature measurements of biological tissues in close to in vivo conditions are presented. The study is based on the correlation of the temperature inside the sample with the deviation in the luminescent spectra of heat-sensitive upconversion [Y2O3: Yb, Er] particles administered into the biological tissue. The linear temperature dependence of the red/green luminescence ratio of the in-tissue embedded particles was observed. Temperature control of the sample was carried out using a digital multimeter with a thermocouple.

To determine local temperature of a biological tissue, we used the commercially available [Y2O3:Yb, Er] upconversion nanoparticles (PTIR660-UF, Phosphor Technology, UK) with the particle size ~1.6 μm.

The aim of this work is to study the possibility of retrieval of the real temperature inside the biological tissue in the vicinity of the [Y2O3:Yb, Er] upconversion nanoparticle (UCPs) location from luminescence spectra of the particles.

Interest for the use of UCNPs in comparison to other particles increases due to their high photochemical stability, low toxicity [1] and stable narrow-band emission upon excitation in the tissue transparency window. UCP fluorescent photons have higher energy than the photons of excitation radiation. This leads to the fact that autofluorescence of biological tissues is extremely low in the spectral region of UCP fluorescence eliminating the fluorescent background of the biological tissue [2].

Heating a biological tissue during photothermolysis is most often monitored by measuring the surface temperature by noncontact method using a thermal imager or the internal temperature at certain points by thermocouples. However, during these measurements, the impossibility of complete control of processes of heat transfer and propagation of laser radiation in the biological tissue leads to the ambiguity of internal temperature retrieval from obtained distribution of the surface temperature. This complicates the performance of the controlled photothermolysis. Therefore, real-time measuremenst of the spatial distribution of temperature inside biological objects directly in the course of photothermolysis is important.

Temperature dependence of the peak position in fluorescence spectra of water suspensions of [Y_2O_3:Yb, Er] particles located in a biological tissue was recorded. Chicken muscle (the sample thickness was 2.5 mm) tissue was used for specimens. Water suspension of [Y_2O_3:Yb, Er] particles was applied to the surface of the tissue sample, which then was kept for 20 min in order for the particles to penetrate deep into the sample. To simulate the conditions of signal recording from the depth of the biological tissue, the sample with embedded particles was covered with a similar one. For heating, the sample of biological tissue was placed on a heating element, whose temperature determined by a thermocouple was varied from 25 to 70 °C. The samples were kept at each temperature for 5 min.

During the heating of the tissue, its intrinsic luminescence usually decreases [3]. In addition, the muscle tissue shields effectively both luminescence and excitation light due to absorption and scattering. Therefore, during the heating, the formation of the luminescence band of the UCNPs in the region of 530 nm, as described in our paper [4, 5], is shielded completely by intrinsic luminescence of the tissue. Consequently, as a criterion of heating, we have chosen the ratio of the intensities of the luminescence peaks of the biological tissue and the upconversion particles [5].
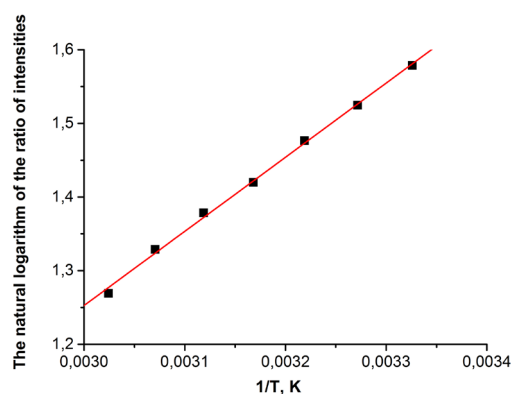
Fig. 1. Temperature dependence of the ratio of the luminescence intensity at 551- and 524-nm wavelengths for muscle tissue with UCP inside. The excitation wavelength is 975 nm.

It is shown that under excitation by the 975 nm-laser, skin autofluorescence in the spectral region of the nanoparticle fluorescence is absent.The ratio of the intensities at the peaks of the luminescence spectra of the UCPs is linearly dependent on the temperature of the [Y_2O_3:Yb, Er] particle environment (Fig. 1) making the method promising bulk temperature measurements.

[1] D.K. Chatterjee, Z. Yong, Nanomed. J. 3, 73–82 (2008)
[2] N. Zhou, J. Ni, R. He, Nano Biomed Eng. 5 (3), 131-139 (2013)
[3] D. Barton, Variation of Fluorescence with Temperature in Human Tissue, 63 (2010)
[4] Ju.G. Konyukhova, A.A. Skaptsov, E.K. Volkova, V. Galushka, V.I. Kochubey, Proc. SPIE. 9031, 90310L-1 (2014)
[5] E. Volkova, A. Skaptsov, J. Konyukhova, V. Kochubey, M. Kozintseva, Proc. SPIE 94480, 94480V-6 (2015)

MULTIMODAL COHERENT NONLINEAR RAMAN MICROSPECTROSCOPY BY CHIRPED ULTRASHORT LASER PULSES

A.A.Lanin[1,2], E.A.Stepanov[1,2], R.A.Tikhonov[1], A.B.Fedotov[1,2], A.M.Zheltikov[1-4]

[1]*Faculty of Physics, International Laser Center, Moscow State University, Moscow, 119992 Russia*

[2]*Russian Quantum Center, Moscow State University, Moscow, 119992 Russia*

[3]*Texas A&M University, College Station, TX 77843, USA*

[4]*National Research Centre Kurchatov Institute, Moscow, 123098 Russia Author(s)*

lanin@physics.msu.ru

We demonstrate the physical principles of multimodal nonlinear optical microspectroscopy, integrating methods of coherent and stimulated Raman scattering of ultrashort chirped laser pulses in a single optical scheme. Nonlinear phase distortions of ultrashort laser pulses are accurately compensated within a broad spectral range in this scheme to enable a high spectral resolution laser microspectroscopy that can reliably resolve groups of fingerprint molecular vibrations with close frequencies, thus acilitating an analysis of complex multicomponent systems.

Coherent anti-Stokes Raman scattering (CARS) has been successfully used for in vivo microscopy, providing a high chemical selectivity, subcellular spatial resolution, and high imaging frame rates [1]. Within the past few years, SRS microscopy has been finding growing applications in the microscopy of biological objects [2]. Ultrashort laser pulses inevitably impose limitations on the spectral resolution in nonlinear optical microspectroscopy. However, the coherence of laser pulses suggests attractive solutions to this problem, allowing the spectral resolution of nonlinear microspectroscopy to be substantially improved by pulse chirping [3–5]. A linear chirp defines a one-to-one map relating the frequency to the delay time τ between the laser pulses. With this map defined, the spectrum of a Raman-active mode can be found by measuring the intensity of the nonlinear Raman signal as a function of τ.

We present the results of SRS microspectroscopy experiments performed on molecular vibrations of polystyrene, toluene, and water using transform-limited pulses with a pulse width of about 160 fs (Fig.1). The SRS loss spectra measured in this scheme feature broad bands corresponding to Raman-active vibrations of CH and OH groups of the studied molecules. As can be seen in Fig. 1a, because of the limited spectral resolution (at a level of 100 cm^{-1}), typical of this version of nonlinear optical microspectroscopy, the fine structure of the Raman bands observed in SRS loss spectra remains unresolved. In Fig. 1b, we present the signals of CARS and SRS by molecular vibrations of toluene measured as functions of the delay time τ using pump and Stokes pulses both linearly chirped up to 3.5 ps. Applying the one-to-one map relating the delay time to the frequency detuning from the Raman resonance, defined by the linear chirp of the laser pulses (blue circles and the dash-dotted line in Fig. 1b), we identify the peaks observed in time-resolved nonlinear Raman signals at delay times of 2480, 460, –270, and –1965 fs in Fig. 1b as the Raman modes of toluene with frequencies of 2920, 2983, 3003, and 3056 cm^{-1}.
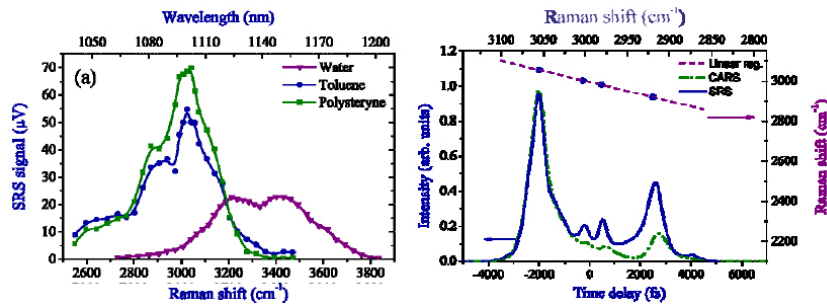
Fig. 1. (a) Spectra of SRS loss recorded for (rectangles) polystyrene, (circles) toluene, and (triangles) water molecules using transform-limited femtosecond pulses. (b) The SRS loss and CARS signals for toluene measured versus the delay time between the laser pulses. The upper scale represents the frequency detuning from the Raman resonance

Phase characterization of ultrashort laser pulses was performed in our experiments by means of cross-correlation frequency resolved optical gating (XFROG) (Fig. 2). Linearly chirped pump and Stokes pulses used in our experiments had pulse widths T_{pu}=3.7 ps and T_{st} = 3.2 ps. The chirp parameter was adjusted by varying the distance between the diffraction gratings in the stretchers in such a way as to achieve the spectral resolution needed in a specific experiment.
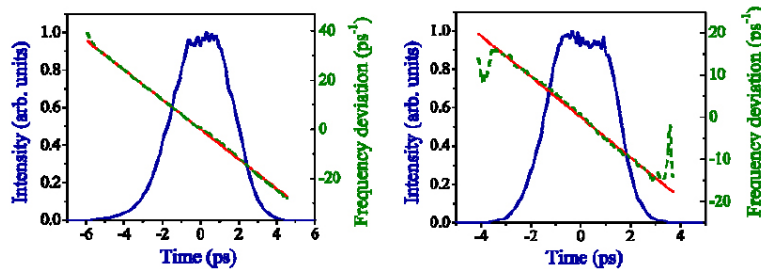
Fig. 2. Temporal envelopes (blue solid lines) and the instantaneous frequency deviations from the central frequencies (dashed lines) retrieved from the XFROG spectrograms for the (a) pump and (b) Stokes pulses.

[1] A. Zumbusch, G. R. Holtom, and X. S. Xie, Phys. Rev. Lett. 82, 4142 (1999).
[2] C. W. Freudiger, W. Min, B. G. Saar, S. Lu, G. R. Holtom, C. He, J. C. Tsai, J. X. Kang, and X. S. Xie, Science 322, 1857 (2008).
[3] A. M. Zheltikov and A. N. Naumov, Quantum Electron. 30, 606 (2000).
[4] T. Hellerer, A. M. K. Enejder, and A. Zumbusch, Appl. Phys. Lett. 85, 25 (2004).
[5] A. A. Lanin, I. V. Fedotov, A. B. Fedotov

IMPROVEMENT OF UPCONVERSION DEEP-TISSUE IMAGING WITH OPTICAL CLEARING

A.P. Popov[1], E.V. Khaydukov[2], A.V. Bykov[1], V.A. Semchishen[1], V.V. Tuchin[3,4], I.V. Meglinski[1]

[1]*Optoelectronics and Measurement Techniques Laboratory, University of Oulu, Oulu, Finland*

[2]*Institute on Laser and Information Technologies, Russian Academy of Sciences, Moscow, Russia*

[3]*Research-Educational Institute of Optics and Biophotonics, Saratov State University, Saratov, Russia*

[4]*Institute of Precise Mechanics and Control of Russian Academy of Sciences, Saratov, Russia*

E-mail: popov@ee.oulu.fi

We report on the deep-tissue imaging using novel upconversion nanoparticles (UCNPs) β-NaYF4:Yb3+:Tm3+ (excitation wavelength: 980 nm, detection wavelength: 800 nm) and glycerol as an optical clearing agent to enhance imaging from under 6-mm-thick porcine muscle tissue samples. We show that improvement of luminescent label visualization is caused by transforming of the diffuse label-emitted light into the direct component. This results in 2-fold increase in visibility (ratio of the sum and difference of the maximal and minimal intensity) of the label, thus making the combination of the phosphors and optical clearing promising for precise detection of tissue-embedded labelled inhomogeneities.

Experimental research on deep-tissue imaging of tissue-mimicking phantoms, thick (6-7 cm) muscle tissue in vitro using novel up-conversion luminophores was performed and enhanced by optical clearing. An original setup (Fig. 1) was constructed for this purpose comprising a diode laser emitting at 980 nm, a dichroic mirror, an optical filter to cut the residual pumping radiation and a CCD camera capable to capture pictures within defined time in certain time intervals. Image processing was done in Matlab environment. Glycerol was used an optical clearing agent enhancing visibility of the embedded luminescent label. Figure 2 shows initial and final appearance of the luminescent label, while Fig. 3 analyses picture visibility and kinetics of optical clearing.

(a)   (b)
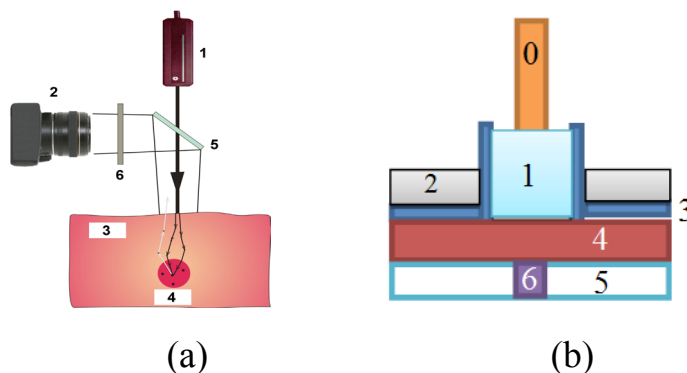
Fig. 3. Outline of the imaging system (a): laser (1), detector (2), tissue (3), inhomogeneity with NALs (4), dichroic mirror (5), filter (6). Design of the sample holder: 0– laser beam (2 mm in diameter); 1 – optical clearing agent, glycerol (0.1 mL); 2 – metal ring; 3 – plastic cover (100-um thick) with a syringe well, 4 – tissue sample (1-mm thick), 5 – transparent phantom (1-mm thick), 6 – luminescent label (2 mm in diameter)

<div align="center">(a)   (b)</div>

Fig. 2. Upconversion luminescence of a star-shaped label @ 800 nm before (a) and after 195 min (b) of glycerol clearing 6-mm-thick porcine muscle tissue in vitro.

<div align="center">(a)   (b)</div>
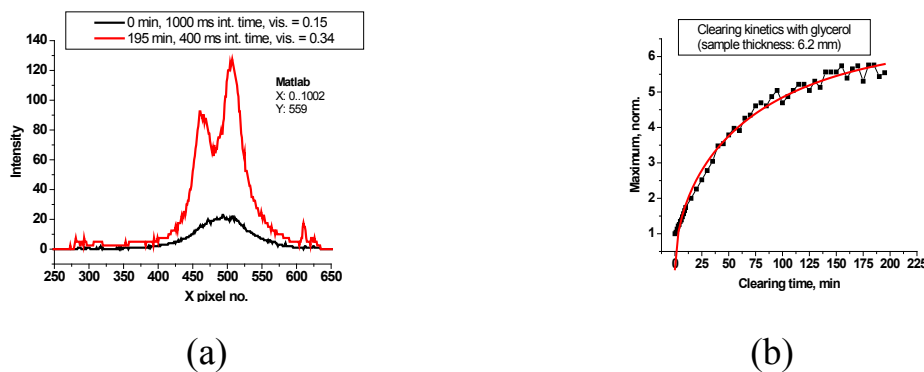
Fig. 3. Comparison between starting and final intensity of the two lower star edges from Fig. 2b (a) and corresponding kinetic clearing curve.

[1]   A.P. Popov, A.V. Bykov, V.I. Sokolov, Y.V. Lysak, A. Nadort, A.V. Priezzhev, R. Myllylä, A.V. ,Zvyagin, "Upconversion luminophores as a novel tool for deep tissue imaging," Proc. SPIE 8090, 80900V (2011).

[2]   E.A. Grebenik, A. Nadort, A.N. Generalova, A.V. Nechaev, V.K.A. Sreenivasan, E.V. Khaydukov, V.A. Semchishen, A.P. Popov, V.I. Sokolov, A.S. Akhmanov, V.P. Zubov, D.V. Klinov, V.Ya. Panchenko, S.M. Deyev, A.V. Zvyagin, "Feasibility study of the optical imaging of a breast cancer lesion labeled with upconversion nanoparticle biocomplexes," J. Biomed. Opt. 18 (7), 076004 (2013).

[3]   E.V. Khaydukov, V.A. Semchishen, V.N. Seminogov, A.V. Nechaev., A.V. Zvyagin, V.I. Sokolov, A.S. Akhmanov, V.Ya. Panchenko, "Visualization of upconverting nanoparticles in strongly scattering media," Biomed. Opt. Express 5(6), 1952-1964 (2014).

[4]   E.V. Khaydukov, V.A. Semchishen, V.N. Seminogov, V.I. Sokolov, A.P. Popov, A.V. Bykov, A.V. Nechaev, A.S. Akhmanov, V.Ya. Panchenko, A.V Zvyagin, "High-contrast fibre-optic visualization of upconverting nanoparticle labels in scattering media," Laser Phys. Lett. 11(9), 095602 (2014).

OPTICAL PROPERTIES OF TISSUES IN THE VISIBLE – NIR SPECTRAL RANGE

Alexey N. Bashkatov, Elina A. Genina, Valery V. Tuchin

Research-Educational Institute of Optics and Biophotonics, Saratov State University, 83 Astrakhanskaya str., Saratov 410012, Russia

Interdisciplinary Laboratory of Biophotonics, Tomsk State University, 36 Lenin Avenue, Tomsk 634050, Russia

a.n.bashkatov@mail.ru

Recent technological advancements in the photonics industry have real progress toward the development of clinical functional imaging, surgical and therapeutic systems. Development of the optical methods in modern medicine has stimulated the investigation of optical properties of human tissues, since the efficacy of optical probing of the tissues depends on the photon propagation and fluence rate distribution within irradiated tissues. There are many diagnostic and therapeutic applications of optical methods, for example, for the monitoring of blood oxygenation and tissue metabolism, detection of malignancies, optical imaging, laser surgery, photodynamic therapy, and etc. For these applications, the knowledge of tissue optical properties is of great importance for interpretation and quantification of the diagnostic data, as well as for prediction of light distribution and absorbed energy at laser therapeutic and surgical use. Numerous investigations related to determination of tissue optical properties are available in literature; however, the optical properties of many tissues have not been studied yet in a wide wavelength range.

In this paper, the tissue optical properties (absorption, scattering and reduced scattering coefficients, and scattering anisotropy factor) measured in vitro by using an integrating sphere spectrometer are presented. We have summarized the optical properties of human eye sclera [1], skin [2], adipose tissue [2, 3], maxillary sinus [2], colon [4], muscle, parietal peritoneum [5], dura mater [6], bone [7], lung, pancreas, nasal polyps, tonsils, and stomach wall mucous measured in the visible – NIR spectral range. Optical models describing wavelength dependence of the tissue optical properties
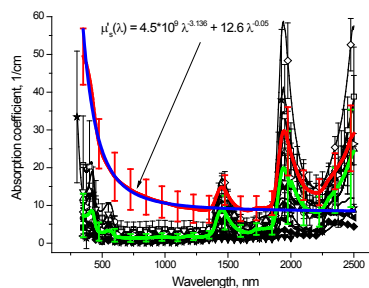
Fig. 1. The absorption spectra of human eye sclera, skin, adipose tissue, maxillary sinus, colon, muscle, parietal peritoneum, lung, pancreas, nasal polyps, tonsils, and stomach wall mucous. The green line corresponds to absorption averaged over all investigated tissues. The red line correspond to wavelength dependence of reduced scattering coefficient averaged over all investigated tissues, and blue line correspond to its approximation by a power law. have been presented.

Figure 1 presents spectra of absorption coefficient of the investigated tissues. It is well seen that tissue absorption has a minimal value in the spectral range from 600 to 1300 nm (2.5±1.5 cm–1) within a so-called "first transparency window (TW)" and from 1650 to 1800 nm (3±1.5 cm–1) in the "second-TW" of tissues. Last time more and more interest attracts the "third-TW"

from 2150 to 2350 nm with absorption coefficient of 2.5 to 15 cm–1, because in this range scattering coefficient is the lowest. Optogenetics and glucose sensing could be beneficial in this wavelength range. In the spectral range 400-600 nm the absorption coefficient increases due to the presence of blood hemoglobin in tissues. Increasing of absorption in the spectral ranges 1350-1600 nm, 1800-2150 nm and 2350-2500 nm deals with absorption of tissue water; and significant variations in the absorption coefficient values is connected with differences in water content in the tissues.

In the spectral range from 400 to 1300 nm scattering properties of the tissues can be approximated by a power law [8]: $\mu'_s(\lambda) = A\lambda^{-w_1} + B\lambda^{-w_2}$, where λ is wavelength (nm), μ'_s is reduced scattering coefficient (cm^{-1}), μ_s is scattering coefficient (cm^{-1}), g is scattering anisotropy factor, and w is wavelength exponent. In the Table 1 we summarized examples of the approximation of scattering properties some tissues.

Tissue	Approximation
Human eye sclera	$\mu'_S(\lambda)=1.848*10^7\lambda^{-1.995}$
Human skin dermis	$\mu'_S(\lambda)=7.059*10^{11}\lambda^{-3.775}+ 7.195\lambda^{-0.027}$
Human subcutaneous adipose tissue	$\mu'_S(\lambda)=1050.6\lambda^{-0.68}$
Human maxillary sinus mucous	$\mu'_S(\lambda)=443742.6\lambda^{-1.62}$
Human stomach wall mucous	$\mu'_S(\lambda)=3.4*10^7\lambda^{-23}+ 20.5\lambda^{-0.14}$
Mucous layer of human colon	$\mu'_S(\lambda)=3.966*10^{10}\lambda^{-3415}+ 538.08\lambda^{-0.611}$
Submucous layer of human colon	$\mu'_S(\lambda)=1.807*10^{10}\lambda^{-3.488}+ 561.89\lambda^{-0.754}$
Parietal peritoneum mucous/submucous layer	$\mu'_S(\lambda)=3.54*10^{10}\lambda^{-3.531}+ 28.42\lambda^{-0.124}$
Parietal peritoneum muscle layer	$\mu'_S(\lambda)=6.623*10^{10}\lambda^{-3.488}+ 44.71\lambda^{-0.393}$

Table 1. The approximation of scattering properties of the investigated tissues in the range 400-1300 nm

[1] A.N. Bashkatov, E.A. Genina, V.I. Kochubey, V.V. Tuchin, Optics and Spectroscopy 109(2), 197-204 (2010).
[2] A.N. Bashkatov, E.A. Genina, V.I. Kochubey, V.V. Tuchin, Journal of Physics D: Applied Physics 38, 2543-2555 (2005).
[3] A.N. Bashkatov, E.A. Genina, V.I. Kochubey, V.V. Tuchin, Optics and Spectroscopy 99(5), 836-842 (2005).
[4] A.N. Bashkatov, E.A. Genina, V.I. Kochubey, V.S. Rubtsov, E.A. Kolesnikova, V.V. Tuchin, Quantum Electronics 44(8), 779-784 (2014).
[5] A.N. Bashkatov, E.A. Genina, M.D. Kozintseva, V.I. Kochubey, S.Yu. Gorodkov, V.V. Tuchin, Optics and Spectroscopy 120(1) (2016) (accepted).
[6] E.A. Genina, A.N. Bashkatov, V.I. Kochubey, V.V. Tuchin, Optics and Spectroscopy 98(3), 470-476 (2005).
[7] A.N. Bashkatov, E.A. Genina, V.I. Kochubey, V.V. Tuchin, Proc. SPIE 6163, 616310 (2006).
[8] A.N. Bashkatov, E.A. Genina, V.V. Tuchin, Tissue Optical Properties / in Handbook of Biomedical Optics, D.A. Boas, C. Pitris, and N. Ramanujam (eds.), (Taylor & Francis Group, LLC, CRC Press Inc., 2011).

OCT 6 2003

OCT 8 2003

OCT 6 2003

OCT 8 2003